https://doi.org/10.5194/egusphere-2026-4960
Preprint. Discussion started: 26 August 2026

Fine Particle Liquid Water and Acidity over North American Cities during the Summer of 2023

Magesh Kumaran Mohan[1], Amy Sullivan[2], Emily Lill[2], Ilana Pollack[2,3], Alison Piasecki[3,4,*], Sarah Albertin[4], Ann Middlebrook[4], Wyndom Chace[3,4], Andrew Rollins[4], Carsten Warneke[4], Steven S. Brown[4], Lu Xu[5], Katherine Ball[6], John D. Crounse[6], Paul O. Wennberg[6], Stelios Kakavas[7], Spyros N. Pandis[7], Athanasios Nenes[7,8], and Rodney J. Weber[1]

[1]Department of Earth and Atmospheric Sciences, Georgia Institute of Technology, Atlanta, GA, USA

[2]Department of Atmospheric Science, Colorado State University, Fort Collins, CO, USA

[3]Cooperative Institute for Research in Environmental Sciences at the University of Colorado, Boulder, CO, USA

[4]NOAA Chemical Sciences Laboratory, Boulder, CO, USA

[5]Washington University, St Louis, MO, USA

[6]California Institute of Technology, Pasadena, CA, USA

[7]Foundation for Research and Technology Hellas, Center for the Study of Air Quality and Climate Change, Department of Chemical Engineering, University of Patras, Patras, Greece.

[8]School of Architecture, Civil and Environmental Engineering, Ecole Polytechnique F´ed´erale de Lausanne (EPFL), Lausanne, Switzerland

*Now at USGS Denver, Colorado

Corresponding author: Rodney J. Weber, rweber@eas.getech.edu

https://doi.org/10.5194/egusphere-2026-4960
Preprint. Discussion started: 26 August 2026

ABSTRACT

Fine aerosol liquid water content (ALWC) and acidity (pH) are co-determined, pH primarily reflects the ratio of hydrogen-ion concentrations in air (H^+_{air}) to ALWC. Inorganic ions dominate H^+_{air} and often ALWC, whereas organic aerosol (OA) mainly adds water. Added OA water, however, shifts gas–particle partitioning of semi-volatile species, altering H^+_{air} itself, and thus pH and the aqueous-phase processes it governs. We characterize PM_1 ALWC and pH over four North American cities using airborne AEROMMA measurements (June–August 2023), including periods influenced by aged wildfire smoke with high OA but little effect on inorganic species. ALWC and pH were predicted with ISORROPIA-Lite, which includes OA water, and evaluated against measured partitioning of NH_3–NH_4^+ and HNO_3–NO_3^-. Predicted ammonia partitioning agreed with observations ($R^2 > 0.75$, within ~±10%), whereas nitrate was systematically over-predicted by ~27%. Outside smoke, inorganic ions dominated ALWC despite being a minor mass fraction; within smoke, organic water dominated (45–65%). Across all cities, pH remained low and varied little (1.5–2.5, 10th–90th percentile). Particle-phase fractions were 0.17–0.56 for NH_4^+ but only 0.1–0.22 for NO_3^-, giving nitrate less redistribution and pH-buffering capacity than NH_4^+. Including OA water raised pH during smoke by at most 0.62 units and improved HNO_3–NO_3^- agreement. Summertime PM_1 acidity thus remains persistently low and thermodynamically stabilized across diverse composition regimes, with wide-ranging implications for regulatory, environmental, and human-health impacts.

https://doi.org/10.5194/egusphere-2026-4960
Preprint. Discussion started: 26 August 2026

1. INTRODUCTION

Atmospheric aerosols (or particulate matter, PM) affect ecosystems, human health, geochemical cycles, and climate. Aerosol acidity (pH) is central to the chemistry underlying these effects because it governs key heterogeneous processes, including the gas–particle partitioning of semi-volatile inorganic species such as ammonium and nitrate (Guo et al., 2016; Nenes et al., 2020), the multiphase oxidation of S(IV) to sulfate (Tanner et al., 2009; Tilgner et al., 2021), and the formation of secondary organic aerosols (SOA) through acid-catalyzed pathways (Surratt et al., 2009). Aerosol pH is tightly coupled to aerosol liquid water content (ALWC), which is determined primarily by hygroscopic inorganic species (Nguyen et al., 2015). Acidity and ALWC are co-determined through their mutual role in affecting the final equilibrium state. Among PM_1 inorganic species, sulfate (the dominant S(VI) component) is a key species: it is nonvolatile, contributes directly to liquid water, and, as a strong acid, exerts a primary control on H^+ concentrations. Nitrate has similar hygroscopicity to sulfate and contributes to H^+ concentration but is semi-volatile and its behavior is more complex with a strong nonlinear dependence on pH. Other salts (e.g., NaCl, KCl, etc.) can be important in certain environments but are generally less significant for PM_1 than $PM_{2.5}$. Ammonia is often the dominant base; it raises pH and affects ALWC through its influence on gas to particle partitioning of semi-volatile hygroscopic species such as nitrate (and chloride in some environments). ALWC is among the largest contributors to particle mass in the atmosphere, often exceeding dry aerosol mass by 2–3 times (Liao and Seinfeld, 2005; Nguyen et al., 2016). It controls the extent of aqueous-phase reactions through reaction volume and influences aerosol optical properties, affecting visibility and the regional to global radiation balance (Pilinis et al., 1989; Phillips et al., 2017; Hennigan et al., 2023). Gas–particle partitioning of semi-volatile nitrogen species, governed jointly by pH and ALWC, alters reactive nitrogen deposition patterns and the overall nitrogen cycle, with consequences for sensitive ecosystems (Nenes et al., 2021). Particle acidity has also been linked to adverse health effects (Song et al., 2024), including the enhancement of trace metal dissolution (e.g., Fe and Cu) under acidic conditions (pH < 3–4) (Meskhidze et al., 2003; Oakes et al., 2012; Fang et al., 2017), elevated oxidative stress via interactions with other PM components and oxidant gases (Song et al., 2024), and effects on the viability and infectivity of airborne viruses (Luo et al., 2023; Klein et al., 2022).

https://doi.org/10.5194/egusphere-2026-4960
Preprint. Discussion started: 26 August 2026

Aerosol pH is a state variable of a coupled thermodynamic system, often determined by the overall equilibrium among gas and particle concentrations of mainly inorganic species, along with relative humidity, and temperature. Thermodynamic models, such as ISORROPIA, solve a system of coupled equilibrium equations – Henry's law, acid dissociation, ion charge and mass balance, and activity coefficient relationships – to predict the pH and phase partitioning of semi-volatile species, including water vapor, that simultaneously satisfy all constraints. As a state variable, pH reflects the system's equilibrium position rather than the influence of any single driver. A mechanistic understanding of aerosol thermodynamics can be gained only through investigating the coupled system, and not through analysis of individual aspects, as, for example, has been done when using proxies to characterize particle acidity.

Despite its importance, directly measuring aerosol pH and ALWC without sample alteration remains analytically challenging (Pye et al., 2020; Li et al., 2025). Inferring pH using proxy metrics such as an ion balance has been shown to produce inaccurate predictions on particle acidity and obscures mechanistic understanding, in part because ALWC is not considered (Hennigan et al., 2015; Guo et al., 2015, 2016; Weber et al., 2016; Pye et al., 2020). As a result, thermodynamic equilibrium models have become the primary tool for quantifying aerosol pH and ALWC and to interpret tropospheric aerosol and gas composition data (Guo et al., 2015, 2016; Arangio et al., 2022). These thermodynamic models are integrated into chemical transport models to study pH and ALWC variations across different scales (Lawal et al., 2018; Kakavas et al., 2025). From a global perspective, fine particle pH tends to range from -1 to 5, depending on regional emissions of acidic and basic species (e.g., sulfate, nitric acid, ammonia, organic acids and non-volatile cations), and meteorological conditions. PM_1 pH is generally much lower than the pH of cloud or fog water (Pye et al., 2020). However, in many past studies accurately predicting fine particle pH has been limited by incomplete gas-phase measurements, particularly of ammonia (NH_3) and nitric acid (HNO_3), the key species often governing inorganic aerosol thermodynamics. Measuring both phases constrains model inputs and enables independent evaluation of the equilibrium assumption and model performance through observed gas-particle partitioning (Guo et al., 2015, 2016; Pye et al., 2020). For example, measurements of total (gas+particle) ammonia (TNH_x) and total nitrate (TNO_3) offer a more stringent test of thermodynamic model performance. Thermodynamic model predictions with only particle measurements as input have been shown to

https://doi.org/10.5194/egusphere-2026-4960
Preprint. Discussion started: 26 August 2026

give unreliable results as small measurement errors in aerosol composition produce large errors in predicted gas-particle partitioning predictions (Hennigan et al., 2015).

East–West gradients in fine aerosol composition across the United States have been noted for some time, with sulfate-dominated aerosol in the eastern US and higher nitrate contributions in the western US. These contrasts that have historically been interpreted as evidence of large regional differences in aerosol acidity (Harrison et al., 2000; Hand et al., 2012). However, proxy-based acidity metrics may substantially mischaracterize regional acidity gradients (Hennigan et al., 2015; Weber et al., 2016). These spatial characteristics may be changing as emissions of important precursors, such as sulfur dioxide (SO_2) and nitrogen oxides (NO_x), have substantially decreased, in contrast to the growing influence of wildfires on aerosol composition across North America.

This study characterizes summertime PM_1 ALWC and pH across major North American urban centers and evaluates their influence on the gas–particle partitioning of semi-volatile species. Aerosol composition and gas-phase measurements from the 2023 AEROMMA (Atmospheric Emissions and Reactions Observed from Megacities to Marine Areas) aircraft campaign are used to predict PM_1 ALWC and pH using the thermodynamic model ISORROPIA-Lite which includes the influence of aerosol water taken up by organic species on overall ALWC and pH. Model predictions are evaluated against observed partitioning of nitric acid and ammonia, providing an observational test of thermodynamic model performance for bulk PM_1 pH. The dataset also includes periods affected by the long-range transport of smoke from Canadian wildfires, enabling the assessment of smoke impacts on ALWC and pH. Together, these results provide a thermodynamically based analysis of urban aerosol acidity and liquid water across contrasting North American emission regimes, verified by gas-particle partitioning data.

2. METHODS

2.1. Aircraft Campaign

The Atmospheric Emissions and Reactions Observed from Megacities to Marine Areas (AEROMMA) campaign involved 24 NASA DC-8 aircraft research flights (RF) between June 14

https://doi.org/10.5194/egusphere-2026-4960
Preprint. Discussion started: 26 August 2026

and August 26, 2023 (https://csl.noaa.gov/projects/aeromma/). This study uses data from research flights 10 (RF10) through RF24, which encompass all urban flight tracks shown in Fig. 1a.

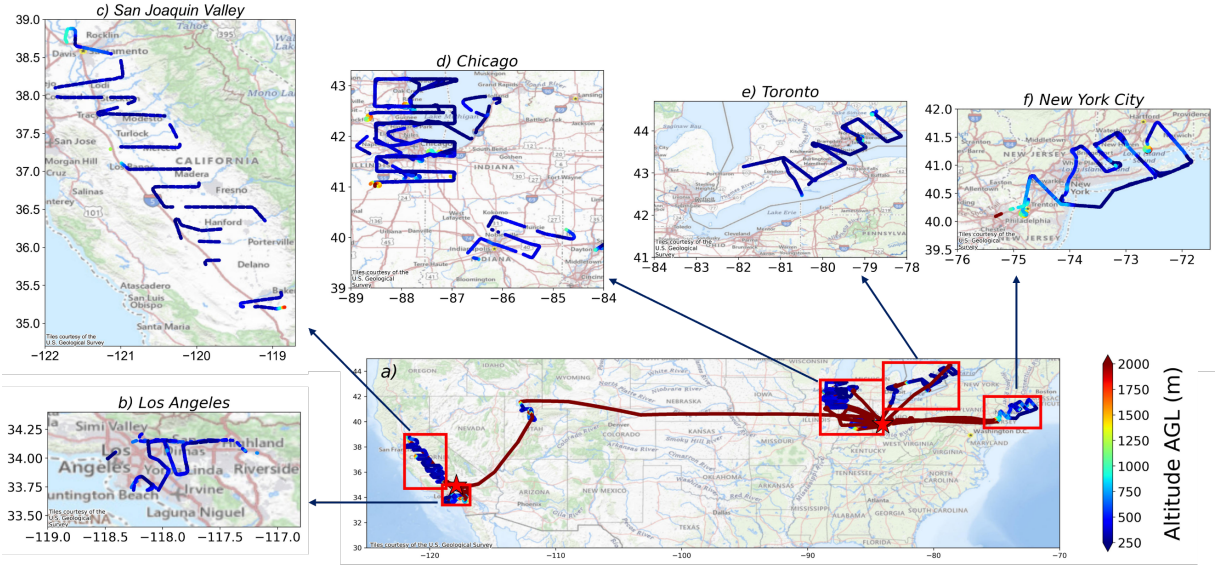

Figure 1. AEROMMA 2023 research flight tracks and study regions. (a) Complete flight tracks from the urban campaign across North America. Combined flight-track segments included in this study over cities – b) Los Angeles (August 23, 25, 26), c) San Joaquin Valley (August 22), d) Chicago (August 1, 2, 8, 12, 15), e) Toronto and Southern Ontario (August 4, 5), f) New York City (July 28, August 9, 16) colored by altitude. Red star markers denote location of aircraft bases. More detailed maps over urban centers are given in the supplementary material (Figs. S7-S11). The base maps were designed and developed by USGS | Powered by USGS (https://basemap.nationalmap.gov/arcgis/rest/services/USGSTopo/MapServer).

Measurements were typically between 11:00 and 19:00 local time across all locations. Targeted flights were made over four major urban centers: New York City (NYC) on July 28, August 9, and August 16; Toronto (TO) on August 4 and August 5; Chicago (CHI) on August 1, 2, 8, 12, and 15, and Los Angeles (LA) on August 23, 25, and 26 (Note, the July 26 NYC flight is omitted because AMS data were unavailable). Data were also collected over intensively managed agricultural rural regions, including the California San Joaquin Valley (SJV) on August 22 and Southern Ontario (SON) enroute to Toronto. Sampling primarily occurred at low altitudes, with a mean aircraft altitude of approximately 700 m over urban areas to capture near-surface boundary layer conditions. Vertical profiles reached altitudes of 3–5 km, typically lasting under five minutes

https://doi.org/10.5194/egusphere-2026-4960
Preprint. Discussion started: 26 August 2026

and repeated 2–6 times per flight. The following analysis focuses on measurements within the boundary layer, estimated from vertical profiles of potential temperature and CO (Chace et al., 2025). We use the boundary layer classification flag developed for the campaign, which can be found in the data archive.

The summer of 2023 was characterized by widespread wildfires across Canada. Smoke from these fires affecting eastern North America during the campaign primarily originated from the Northwest Territories, with contributions from northern Quebec (Jain et al., 2024) and the following analysis includes low/no-smoke versus smoke conditions. Thermodynamic calculations were done at ambient conditions, so all measurements reported at standard conditions were converted to ambient temperature and pressure.

2.2. Instruments

Aerosol Composition: AMS. Non-refractory PM_1 composition was measured by a high-resolution time-of-flight aerosol mass spectrometer (HR-ToF-AMS, Aerodyne Research Inc.; hereafter "AMS") (DeCarlo et al., 2006). Particles were sampled through an NCAR High-Performance Instrumented Airborne Platform for Environmental Research (HIAPER) Modular Inlet (HIMIL), at a standard flow rate of 9 sL min^{-1} (below 9 km altitude) and 15 sL min^{-1} (above 9 km) (Guo et al., 2021), with a pressure-controlled inlet maintaining a constant mass flow rate into the instrument (Bahreini et al., 2008). Data were acquired at 1 Hz on a 1 minute cycle consisting of 6 s background and 46 s ambient measurements. Chemical composition dependent AMS collection efficiency was calculated for each measurement using the algorithm from Middlebrook et al. (2012). Detection limits for the AEROMMA campaign were 0.04 µg sm^{-3} for sulfate and nitrate, 0.02 µg sm^{-3} for ammonium, 0.03 µg sm^{-3} for chloride, and 0.41 µg sm^{-3} for OA. Measurement uncertainties were ±34% for nitrate and ammonium, ±36% for sulfate and non-refractory chloride, and ±38% for OA (Bahreini et al., 2009).

NH_3: QC-TILDAS. Gas-phase NH_3 was measured at 1 Hz using an Aerodyne Quantum Cascade Tunable Infrared Laser Direct Absorption Spectrometer (QC-TILDAS), equipped with an aircraft injection inlet, a filter-less aerodynamic particle separator, and active continuous passivation of sampling surfaces using 1H,1H-perfluorooctylamine. Sampling surfaces were heated to 40°C to minimize NH_3 adsorption. Detailed operation for aircraft measurements is described in Pollack et

https://doi.org/10.5194/egusphere-2026-4960
Preprint. Discussion started: 26 August 2026

al. (2019), and details of the specific AEROMMA DC-8 setup are provided in Lill et al. (2025). Measurement uncertainty is ±12%.

HNO_3: HToF CIMS. Gas-phase HNO_3 concentrations were measured at 1 Hz using the California Institute of Technology High-Resolution Time-of-Flight Chemical Ionization Mass Spectrometer (HToF-CIMS), employing CF_3O^- ion chemistry (Crounse et al., 2006). Aerosol dynamic calculations suggest particles larger than 0.3 μm are excluded from the measurement. Positive artifacts from volatilization of ammonium nitrate aerosol in the inlet and sample line are expected to be minor. Measurement uncertainty is ±25 pptv (uncertainty in the zero) with a potential systematic bias of +20% mainly due to calibration and water dependence.

Other Measurements. Instrumentation used to obtain data also used in this analysis are discussed in the supplement and include: PILS-IC measurements of K^+, UHSAS size-resolved particle volume, and refractory black carbon mass (rBC) concentrations, and gas phase NO, NO_2 and O_3 concentrations. Relative humidity (RH) was derived from water vapor mixing ratio measurements made by a Diode Laser Hygrometer (DLH) with an uncertainty of ±15%. Air temperature was measured by a Rosemount 102 type de-iced probe with a measurement uncertainty of ±0.5 °C. Aircraft coordinates were provided by the DC-8 aircraft data system.

2.3. Thermodynamic Model

Equilibrium aerosol liquid water content (ALWC) and inorganic aerosol composition, including H^+ concentration and the semi-volatile gas species, HNO_3 and NH_3, were predicted using the thermodynamic model ISORROPIA-Lite (http://isorropia.epfl.ch). ISORROPIA-Lite is an updated, computationally efficient version of ISORROPIA-II (Fountoukis and Nenes, 2007) that incorporates organic aerosol mass (OA) contributions to predict OA-associated water uptake and its effect on the equilibrium state. OA-associated water is treated as part of a single bulk aqueous phase in which all inorganic equilibria are solved, so its inclusion affects semi-volatile partitioning, inorganic ion concentrations, and inorganic water uptake. This couples the OA and inorganic systems instead of treating them as additive contributions to total ALWC (Kakavas et al., 2022). The model also provides species-resolved ALWC contributions by individual inorganic components. The model was run in forward mode assuming a metastable aerosol state with no solid precipitates. Model inputs for semi-volatile inorganic species included the measured total (gas + particle) concentrations of nitrate ($TNO_3 = HNO_3 + NO_3^-$) and ammonium ($TNH_x = NH_3 +$

https://doi.org/10.5194/egusphere-2026-4960
Preprint. Discussion started: 26 August 2026

NH_4^+), while non-volatile species such as SO_4^{2-} were input as PM_1 concentrations only, since their gas-phase component is negligible and all S(VI) species are measured as sulfate. To satisfy the metastable assumption, only data with ambient RH > 40% were used (Guo et al., 2016); this criterion excluded 15% of the urban campaign data (15,905 out of 105,621 one-second measurements).

Particle pH was calculated from ISORROPIA-Lite predictions of particle hydronium ion concentration per volume of air (H^+_{air}) and predicted total aerosol liquid water (W):

$$pH = -log_{10}(\gamma_{H^+} H^+_{air}) = -log_{10}\frac{1000\,\gamma_{H^+} H^+_{air}}{W} = -log_{10}\frac{1000\,\gamma_{H^+} H^+_{air}}{W_i + W_o} \quad (1)$$

where W, W_i, W_o and H^+_{air} are concentrations in air in μg m^{-3}. H^+_{aq} (mol L^{-1}) is the hydronium ion concentration in bulk liquid solution, and γ_{H^+}, the H^+ activity coefficient, is assumed to be unity. W_i is the inorganic ALWC and W_o is the OA-associated ALWC. Throughout this study, W_o is determined from an assumed constant OA particle density (ρ_{OA} = 1.3 g cm^{-3}) and hygroscopicity (κ_{OA} = 0.1), based on standard values reported for ambient OA (Petters and Kreidenweis, 2007). We use the bulk approach here, as it requires only routinely available OA properties and is a more straightforward analysis. The model assumes thermodynamic equilibrium conditions; other studies have shown equilibrium is reached on time scales of minutes (Fountoukis et al., 2009). Determining bulk PM_1 pH also assumes internal mixing of various PM_1 components. The validity of these assumptions is assessed by comparing measured and modeled partitioning of semi-volatile species. In summary, the data inputs to the model are TSO_4 (sulfate), TNO_3, TNH_x, OA, ρ_{OA}, κ_{OA}, T and RH.

The NH_3/NH_4^+ and HNO_3/NO_3^- partitioning fractions, defined as $\varepsilon(NH_4^+) = NH_4^+/(NH_4^+ + NH_3)$ and $\varepsilon(NO_3^-) = NO_3^-/(NO_3^- + HNO_3)$, respectively, were calculated directly from the measured and ISORROPIA-Lite-predicted gas- and particle-phase concentrations. To relate these partitioning fractions to predicted aerosol pH and construct the corresponding thermodynamic "S-curves," $\varepsilon(NH_4^+)$ and $\varepsilon(NO_3^-)$ were also computed from the following equilibrium expressions (Guo et al., 2017; Nah et al., 2018), using the ISORROPIA-Lite-predicted activity coefficients, ALWC, and pH:

https://doi.org/10.5194/egusphere-2026-4960
Preprint. Discussion started: 26 August 2026

$$\varepsilon(NH_4^+) = \frac{\left(\frac{\gamma_{H+}}{\gamma_{NH_4^+}}\right) H^*_{NH3} 10^{-pH}\, ALWC\, RT \times 0.987 \times 10^{-14}}{1 + \left(\frac{\gamma_{H+}}{\gamma_{NH_4^+}}\right) H^*_{NH3} 10^{-pH}\, ALWC\, RT \times 0.987 \times 10^{-14}} \quad (2)$$

$$\varepsilon(NO_3^-) = \frac{H^*_{HNO3}\, ALWC\, RT \times 0.987 \times 10^{-14}}{\gamma_{H+}\, \gamma_{NO_3^-}\, 10^{-pH} + H^*_{HNO3}\, ALWC\, RT \times 0.987 \times 10^{-14}} \quad (3)$$

where H^*_{NH3} (atm^{-1}) and H^*_{HNO3} (mole^2 kg^{-2} atm^{-1}) are the equilibrium constants of combined dissolution and dissociation processes for NH_3 and HNO_3, respectively (effective Henry's Law constants), γ_{H^+}, $\gamma_{NH_4^+}$ and $\gamma_{NO_3^-}$ are single-ion activity coefficients for H^+, NH_4^+ and NO_3^-, respectively, R is universal gas constant and T is temperature.

3. RESULTS

3.1. Measurement Results

3.1.1. Overview and Conditions

High-frequency AMS measurements of PM_1 SO_4^{2-}, NO_3^-, NH_4^+, and OA are used as the main PM_1 compositional input to ISORROPIA-Lite to predict ALWC and pH. The AMS does not directly measure the specific inorganic ion concentrations required for this analysis (e.g., SO_4^{2-}, NO_3^-, and NH_4^+). For example, the measurement can include additional organosulfate and organonitrate species. An ion molar balance between NH_4^+ and $(2SO_4^{2-} + NO_3^-)$ within 4% (Fig. S1) demonstrates consistency between the anions and cation and that they are likely reasonable approximations for these ion concentrations.

As a cross-validation on the magnitude of the measurements, total PM_1 mass concentration (sum AMS species + SP2 rBC) is compared with particle volume concentration data providing a density-based assessment of associated uncertainties in predicted ALWC and pH (see Sect. S1 for details). The predicted mass and measured volume are highly correlated (R^2=0.91, see Fig. S1c) and the slope of mass to volume gives an average PM_1 density of 2.1 g cm^{-3}, higher than a more typical density of ~1.4 g cm^{-3}, resulting in the AMS data being approximately 50% higher than the volume measurements. We concluded that there are no specific reasons to support correcting the archived AMS data. Therefore, we use the reported AMS data in the following analysis. We note

https://doi.org/10.5194/egusphere-2026-4960
Preprint. Discussion started: 26 August 2026

applying a 0.67 (=1.4/2.1) factor to all AMS data had little effect on predicted pH but would systematically lower ALWC by ~40%. Furthermore, we note that the best agreement between measured and predicted NH_3/NH_4^+ and HNO_3/NO_3^- partitioning is found for the unaltered AMS data, likely related to the assumption of constant density.

Prior work has shown that non-volatile cations (NVCs) are present at low concentrations in PM_1 and have negligible effects on PM_1 ALWC and pH (Guo et al., 2017) and so they are not considered here, and the partitioning analysis supports this assumption. Potassium (K^+), however, can be a significant PM_1 constituent in biomass burning plumes (Cahill et al., 2008), co-emitted with Cl^- as KCl from wildfires (Reid et al., 2005). Median PILS K^+ concentrations during smoke-impacted flights ranged from 0.05 to 0.22 μg m^{-3}, and sensitivity tests examining its effects on model performance, ALWC, and pH are discussed where relevant below and extensively in the supplement.

3.1.2. Data selection and smoke classification

Data used in this study were selected to represent summertime boundary layer conditions across major population centers in North America sampled during the AEROMMA 2023 campaign. Flight tracks included Greater New York (NYC), Chicago Metro area (CHI; including Indianapolis during transit on 8 August and Gary, Indiana), Greater Toronto area (TO; including Hamilton) and Southern Ontario (SON), Greater Los Angeles (LA), and the California San Joaquin Valley (SJV) (Figs. 1b-e). The urban analyses are based predominantly on measurements over metropolitan areas, although some suburban and industrial regions were also sampled along the flight tracks and are included in the urban dataset because their thermodynamic characteristics were generally similar to the broader urban environment. Rural regions (SON and SJV) are treated separately throughout the analysis.

Several targeted measurements were excluded to maintain a focus on representative regional conditions. These include sampling over southern SJV and over large farms (dairies) in SON, which yielded unique datasets for more focused investigation in subsequent studies (identified as unique events in Fig. 2). Extensive marine sampling near LA was also excluded because it was not representative of the urban atmosphere considered here. In addition, approximately one hour of post-sunset observations collected on 26 August, the only nighttime

https://doi.org/10.5194/egusphere-2026-4960
Preprint. Discussion started: 26 August 2026

282 measurements during the campaign, were excluded because RH remained below the threshold
283 applied in this study (RH > 40%).

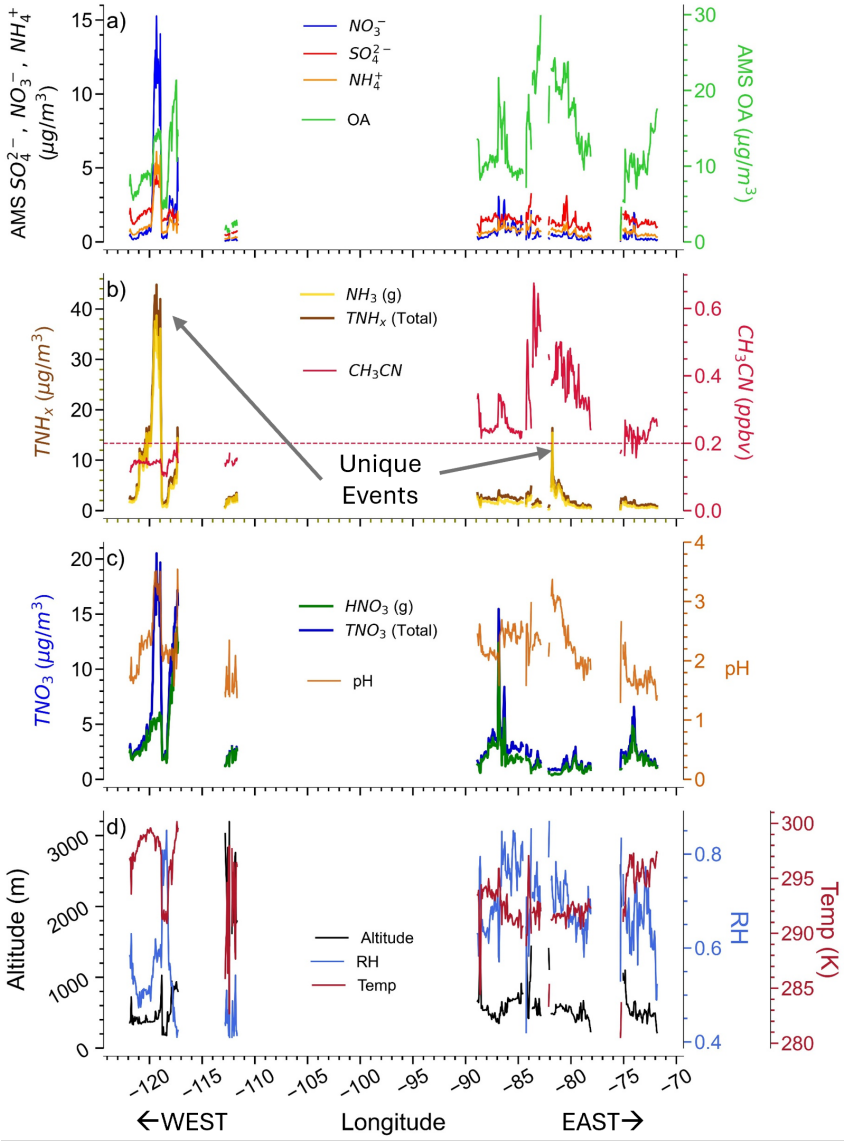

Figure 2. Boundary layer aircraft measurements averaged over 0.05° longitude and plotted west to east. a) reported AMS inorganic species mass on left and OA mass on right axis, b) TNH_x, gas phase NH_3 on left and CH_3CN (dashed line denotes smoke cutoff) on right axis, c) TNO_3, gas phase HNO_3 on left and predicted pH on right axis, d) METNAV Altitude AGL on left and RH and Temperature on right axis. Unique events marked by grey arrow.

https://doi.org/10.5194/egusphere-2026-4960
Preprint. Discussion started: 26 August 2026

The summer 2023 campaign was substantially influenced by widespread wildfire smoke from Canada, primarily originating from the Northwest Territories (Jain et al., 2024; Chen et al., 2025). Following the smoke designation method of Lill et al. (2025), entire research flights were classified as smoke impacted if either (1) the mean boundary layer CH_3CN concentrations exceeded 200 ppt or (2) a medium-to-heavy NOAA Hazard Mapping System (HMS) smoke plume overlapped the flight area. Flights not meeting the criteria were classified as low/no-smoke. This smoke distribution was geographically located mostly in the eastern cities; of the ten flights over NYC, CHI, and TO, only two – August 12 (CHI) and August 16 (NYC) – were designated low/no-smoke, while all flights over LA and SJV occurred under low/no-smoke conditions. All TO flights were smoke impacted. Among the rural areas sampled, SON was also predominantly affected by wildfire smoke, whereas the California SJV was not. For the smoke impacted flights, CH_3CN remained elevated across the sampled regions rather than only during brief plume encounters (Fig. 2), while HMS maps also showed widespread smoke coverage across the corresponding flight areas. Because the smoke was estimated to be more than two days old, the observed effects may not represent those of fresher wildfire smoke and cannot be generalized.

Accordingly, the results presented here are intended to provide a regional-scale overview of aerosol thermodynamics under typical summertime conditions in North American midlatitudes rather than attributing observations to specific emission sources or localized events. Figure 1a shows the complete flight tracks from the urban campaign, whereas Figs. 1b–e show the flight-track segments included in this study. Figure 2 summarizes boundary layer gas-phase and aerosol concentrations, meteorological conditions, and smoke tracers as a function of longitude spanning the breadth of the continent; key boundary layer statistics are reported in Table 1.

3.1.3. Overall contrast East vs. West

Large-scale compositional and meteorological differences across the continent are shown in Fig. 2. Here we broadly divide the continental USA as East and West, based on the measurement gap in the middle of continent, as seen in Fig. 2. East includes Chicago and everything to the east coast, West is mainly California (see Fig. 1). The prevalence of wildfire smoke in the eastern cities and its absence in California is evident from the spatial contrast in the biomass burning tracer (e.g., CH_3CN) and OA concentrations. Even in low/no smoke conditions, OA was the largest component of PM_1 mass in all regions, ranging from 68 to 75% under low/no-smoke conditions and 78 to 90%

https://doi.org/10.5194/egusphere-2026-4960
Preprint. Discussion started: 26 August 2026

under smoke-impacted conditions (Table 2). In the following, East to West differences is assessed using only low/no-smoke flights, since smoke-impacted flights never occurred over California during AEROMMA.

Table 1. Categorical summary of measurements and model results from the AEROMMA aircraft campaign. Boundary layer mean and 1-sd of the data are reported for each category.

Location	Eastern North America						California	
	Urban					Rural	Urban	Rural
	New York City		Chicago		Toronto	Southern Ontario	Los Angeles	San Joaquin Valley
Smoke/ No smoke	no smoke	smoke	no smoke	smoke	smoke	smoke	no smoke	no smoke
Measured Values								
RH	83 ± 7 %	59 ± 11 %	66 ± 11 %	67 ± 11 %	65 ± 10 %	72 ± 6 %	55 ± 10 %	52 ± 6 %
Temp (K)	293 ± 2	296 ± 3	293 ± 2	294 ± 3	292 ± 2	292 ± 1	297 ± 2	297 ± 3
Altitude AGL (m)	499 ± 301	524 ± 306	383 ± 243	330 ± 199	311 ± 177	313 ± 46	360 ± 125	438 ± 331
AMS PM_1 (μg m^{-3})	9.32 ± 5.21	14.79 ± 3.49	5.31 ± 1.49	15.05 ± 3.91	14.91 ± 6.04	24.7 ± 5.45	21.64 ± 7.94	12.34 ± 5.82
SO_4^{2-} (μg m^{-3})	1.58 ± 0.55	1.29 ± 0.58	0.84 ± 0.32	1.71 ± 0.85	0.98 ± 0.67	1.61 ± 1.07	2.01 ± 0.63	1.91 ± 0.76
OA (μg m^{-3})	6.13 ± 3.04	12.84 ± 3.46	3.90 ± 1.11	11.95 ± 3.27	13.27 ± 5.11	21.74 ± 4.32	15.59 ± 5.87	8.13 ± 2.85
SO_4^{2-}/NO_3^- (mol mol^{-1})	6.17 ± 9.29	6.56 ± 7.48	5.01 ± 7.19	3.33 ± 3.17	5.09 ± 7.04	2.46 ± 1.92	1.12 ± 1.28	2.92 ± 3.24
AMS NO_3^- (μg m^{-3})	0.79 ± 1.55	0.19 ± 0.22	0.22 ± 0.26	0.59 ± 0.73	0.22 ± 0.3	0.50 ± 0.37	2.55 ± 2.24	1.20 ± 1.92
HNO_3 (g) (μg m^{-3})	3.40 ± 2.75	1.55 ± 0.88	1.47 ± 0.66	2.81 ± 2.15	1.08 ± 0.79	0.98 ± 0.53	7.84 ± 3.42	3.23 ± 1.37
TNO_3 (μg m^{-3})	4.19 ± 3.91	1.74 ± 0.99	1.68 ± 0.79	3.4 ± 2.66	1.30 ± 1	1.48 ± 0.8	10.39 ± 4.61	4.43 ± 2.72
ε(NO_3^-)	12 ± 12 %	11 ± 7 %	12 ± 10 %	18 ± 12 %	15 ± 9 %	34 ± 13 %	22 ± 14 %	20 ± 17 %
AMS NH_4^+ (μg m^{-3})	0.79 ± 0.58	0.47 ± 0.24	0.35 ± 0.13	0.79 ± 0.37	0.42 ± 0.29	0.83 ± 0.4	1.42 ± 0.8	1.07 ± 0.8
NH_3 (g) (μg m^{-3})	0.54 ± 0.27	0.89 ± 0.6	1.77 ± 0.64	1.71 ± 0.73	0.64 ± 0.31	2.36 ± 1.66	4.78 ± 1.69	9.27 ± 8.25
TNH_x (μg m^{-3})	1.33 ± 0.77	1.37 ± 0.8	2.12 ± 0.69	2.49 ± 0.94	1.06 ± 0.53	3.19 ± 1.71	6.20 ± 2.12	10.34 ± 8.84
ε(NH_4^+)	56 ± 12 %	35 ± 8 %	17 ± 7 %	31 ± 10 %	37 ± 10 %	29 ± 16 %	22 ± 8 %	13 ± 8 %
Thermodynamic Predictions								
PM_1 ALWC (μg m^{-3})	10.31 ± 14.47	3.05 ± 2.68	2.10 ± 1.88	5.98 ± 11.96	4.06 ± 4.77	7.62 ± 4.09	5.01 ± 3.79	2.87 ± 2.43
$(NH_4)_2SO_4$ (μg m^{-3})	3.78 ± 2.48	1.28 ± 0.96	0.99 ± 0.58	2.10 ± 4.45	1.23 ± 1.31	2.19 ± 1.78	1.67 ± 1.08	1.39 ± 0.72
NH4NO3 (μg m^{-3})	3.66 ± 10.51	0.16 ± 0.97	0.34 ± 0.77	1.11 ± 4.33	0.36 ± 1.57	0.80 ± 0.91	1.82 ± 2.24	0.75 ± 1.48
OA LWC (μg m^{-3})	2.87 ± 2.32	1.61 ± 1.1	0.77 ± 0.64	2.69 ± 4.91	2.46 ± 2.23	4.62 ± 1.91	1.52 ± 0.75	0.73 ± 0.38
pH	1.84 ± 0.33	1.64 ± 0.32	2.04 ± 0.36	2.17 ± 0.33	1.96 ± 0.32	2.63 ± 0.35	2.09 ± 0.59	2.22 ± 0.53
pH w/o OA	1.65 ± 0.36	1.12 ± 0.39	1.75 ± 0.33	1.77 ± 0.3	1.34 ± 0.34	2.02 ± 0.32	1.78 ± 0.49	1.94 ± 0.52
ΔpH due to OA LWC	0.19 ± 0.18	0.53 ± 0.15	0.3 ± 0.16	0.41 ± 0.22	0.62 ± 0.12	0.61 ± 0.18	0.31 ± 0.71	0.28 ± 0.39

Mean temperatures were similar across all regions, but California was notably drier during the campaign, with mean RH approximately 17% lower there (58%) compared to the eastern cities (75%). Despite this, average PM_1 mass concentrations were 2–4 times higher in California (Table 1). Among inorganic species, sulfate dominated across all regions (~10–20% of total PM_1 mass),

https://doi.org/10.5194/egusphere-2026-4960
Preprint. Discussion started: 26 August 2026

but generally more so over the eastern cities. Nitrate accounted for 3–8% of total PM_1 mass, with lower contributions in the eastern cities (3% in both NYC and CHI) but notably higher in LA (8%) (Table 2). The mean SO_4^{2-}/NO_3^- molar ratios were 6.17, 5.01, and 1.12 (mass ratios of 9.40, 7.63 and 1.70) for NYC, CHI, and LA, respectively. TNH_x was 3–4 times higher over California and TNO_3 approximately twice as high (Fig. 2; Table 1). These East–West contrasts in aerosol composition are consistent with historical observations (Harrison et al., 2000; Hand et al., 2012; Nguyen et al., 2016).

Table 2. Summary of mean fractional species contributions to PM_1 aerosol liquid water content (ALWC) and PM_1 mass concentration across AEROMMA flight regions, stratified by smoke condition.

City	Condition	ALWC mass fraction (%)			PM_1 mass fraction (%)			
		$(NH_4)_2SO_4$	NH_4NO_3	OA	SO_4^{2-}	NO_3^-	OA	NH_4^+
NYC	no smoke	56	11	33	20	3	68	9
	smoke	38	1	61	8	1	88	3
CHI	no smoke	56	6	38	16	3	74	7
	smoke	50	9	41	12	3	79	6
TO	smoke	31	3	66	6	1	90	3
SON	smoke	26	8	66	5	2	90	3
LA	no smoke	41	23	36	10	9	75	7
SJV	no smoke	59	11	30	16	5	71	8

NYC: New York City, CHI: Chicago, TO: Toronto, SON: Southern Ontario agricultural regions southwest of TO, LA: Los Angeles, SJV: California San Joaquin Valley agricultural region.

3.1.4. City-level contrasts under low/no-smoke conditions

The regional contrasts extend to the city-level data. Total PM_1 was highest in LA (21.64 ± 7.94 μg m^{-3}), followed by NYC (9.32 ± 5.21 μg m^{-3}) and CHI (5.31 ± 1.49 μg m^{-3}). TNO_3 was highest in LA (10.39 ± 4.61 μg m^{-3}), moderate in NYC (4.19 ± 3.91 μg m^{-3}), and lowest in CHI (1.47 ± 0.79 μg m^{-3}), consistent with elevated vehicular NO_x and oxidant levels favoring HNO_3 production, with mean NO_x concentrations up to 5 times higher in LA (Table S1). Despite this wide range in TNO_3, measured nitrate gas/particle partitioning $\varepsilon(NO_3^-)$ was low and relatively similar across all three cities (12%, 12%, and 22% for NYC, CHI, and LA, respectively), meaning nitrate was predominantly in the gas-phase (Fig. 3). TNH_x followed the same ordering as PM_1: LA (6.20 ± 2.12 μg m^{-3}) > CHI (2.12 ± 0.69 μg m^{-3}) > NYC (1.33 ± 0.77 μg m^{-3}), broadly consistent

https://doi.org/10.5194/egusphere-2026-4960
Preprint. Discussion started: 26 August 2026

with the importance of vehicles as an NH_3 source (Lill et al., 2025). By contrast, measured ammonia partitioning $\varepsilon(NH_4^+)$ substantially varied across cities; 56% in NYC compared to 17% and 22% in CHI and LA (Fig. 3).

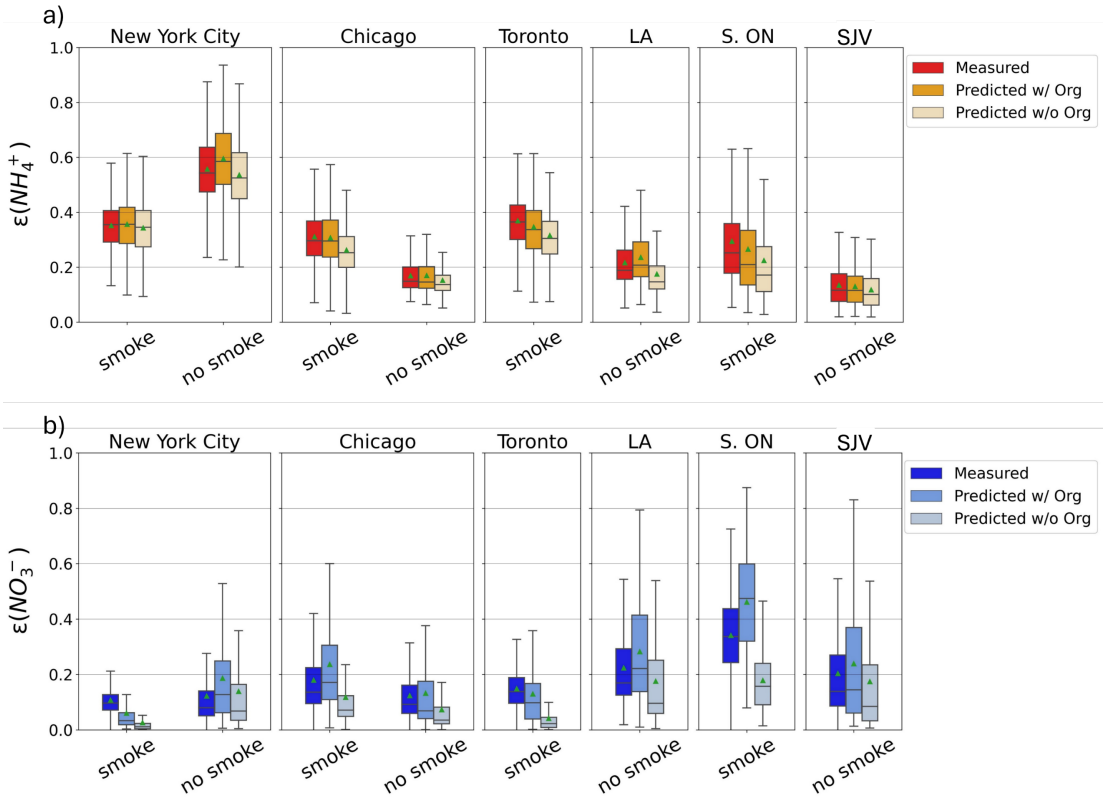

Figure 3. Summary of measured and ISORROPIA-Lite predicted partitioning of (a) ammonium [$\varepsilon(NH_4^+)$] and (b) nitrate [$\varepsilon(NO_3^-)$] across all AEROMMA flights, for two model configurations: with and without including OA contributions.

3.1.5. City-level contrasts under smoke-impacted conditions

In both NYC and CHI, PM_1 during smoke impacted flights were 1.5–3 time higher than during low/no-smoke flights in the same city, driven almost entirely by enhanced OA. The NYC OA/PM_1 mass fraction was 88% during smoke versus 68% for low/no-smoke, CHI OA/PM_1 mass was only slightly higher in smoke, 79% versus 74%. In TO and SON, which was always impacted by smoke, OA/PM_1 was 90% (Table 2). Inorganic PM_1 concentrations showed no consistent

https://doi.org/10.5194/egusphere-2026-4960
Preprint. Discussion started: 26 August 2026

enhancement during smoke (Fig. 4a, b; Table 2). In smoke, sulfate remained the dominant inorganic species, and SO_4^{2-}/NO_3^- molar ratios were unchanged compared to low/no-smoke. Also, no systematic differences in TNO_3 or TNH_x were observed between smoke-impacted and low/no-smoke periods (Table 1 and Fig. 4c, d). This absence of a smoke signal for the inorganic species is evident across the continental transect in Fig. 2, where SO_4^{2-}, TNO_3, and TNH_x remain relatively stable while OA closely tracks CH_3CN. Measured aerosol-phase partitioning was similarly mostly unaffected: $\varepsilon(NO_3^-)$ remained uniformly low (12–22% across all smoke-impacted cities), and while mean $\varepsilon(NH_4^+)$ ranged from 31–37% during smoke flights with no observable shifts attributable to smoke. Overall, smoke substantially elevated OA but produced no systematic change in the measured inorganic species; this lack of an inorganic smoke signal is examined further in Sect. 4.4 and Sect. S5.

3.1.6. Urban–rural contrasts

The California SJV provides a rural reference to contrast LA under comparable temperature and RH conditions. Despite similar $\varepsilon(NO_3^-)$ between the two regions (22 ± 14% in LA and 20 ± 17% in SJV), TNO_3 in the SJV (~4.4 μg m^{-3}) was roughly half that in LA, and total PM_1 in the SJV was lower due to less OA and NO_3^- (Table 1). TNH_x, however, was approximately twice as high in the SJV as in LA, consistent with high agricultural NH_3 sources. In Canada, which was only sampled under smoke conditions, the rural/urban comparison showed that SON had PM_1 NO_3^-, SO_4^{2-}, and OA concentrations 1.5 to 2× higher than TO, and TNH_x approximately 3× higher – again pointing to agricultural emissions of ammonia. $\varepsilon(NH_4^+)$ was similar between SON and TO despite the elevated TNH_x, while there was greater aerosol-phase nitrate partitioning; $\varepsilon(NO_3^-)$ was approximately twice as high in SON (Fig. 3). Together, these urban–rural contrasts highlight the influence of agricultural NH_3 on aerosol thermodynamics.

This measurement comparison has focused on average urban conditions, providing a city-to-city comparison. The high time resolution data allows detailed analysis within each city but is not included here. Within-city variability in meteorological parameters and gas/particle composition along the flight tracks over each of the four cities is discussed in Sect. S2 and maps shown in Figs. S7–S11.

https://doi.org/10.5194/egusphere-2026-4960
Preprint. Discussion started: 26 August 2026

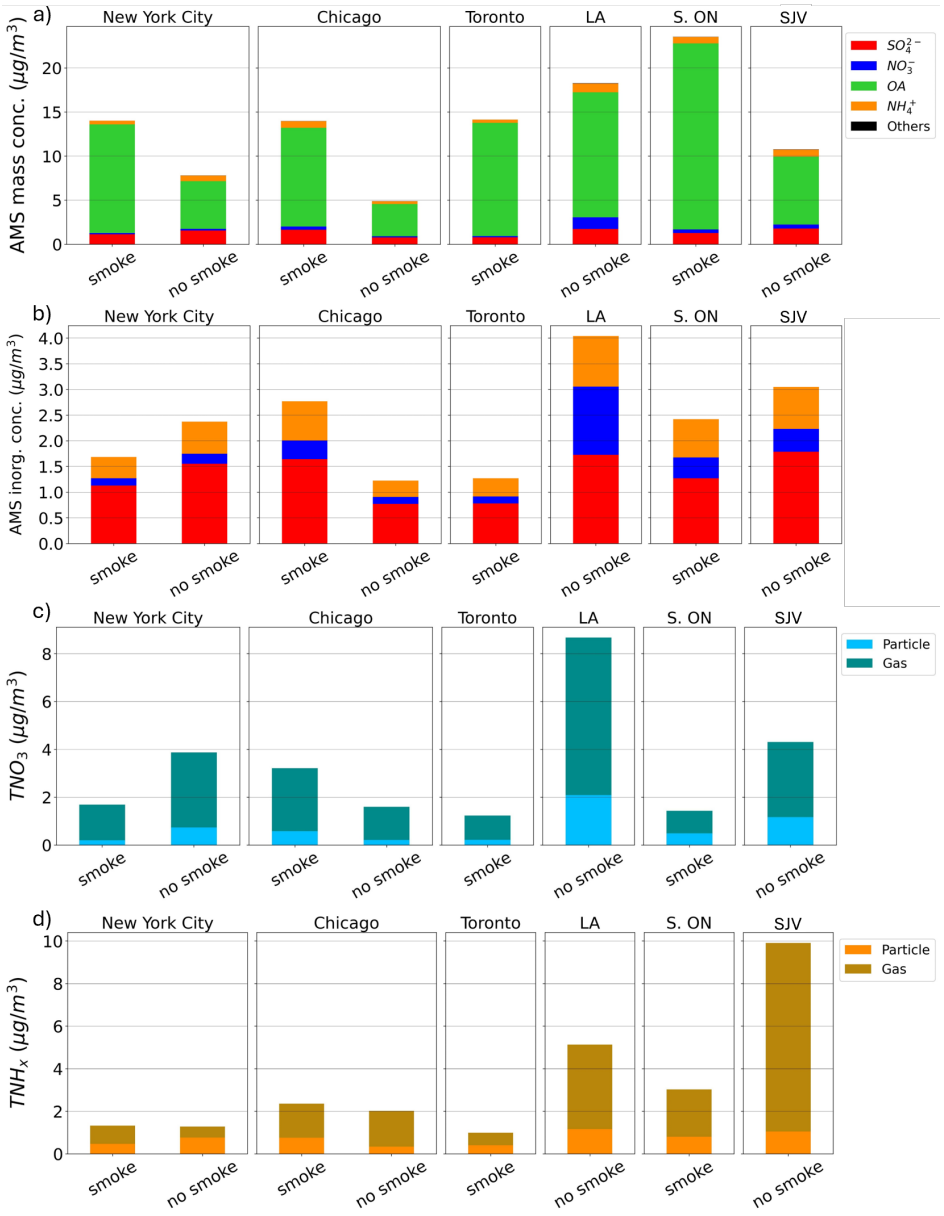

Figure 4. Regional aerosol and gas composition during smoke and low/no-smoke conditions across AEROMMA flight regions. (a) Total PM_1 mass concentration, showing contributions from SO_4^{2-}, NO_3^-, organic aerosol (OA), NH_4^+, and other species. (b) Inorganic PM_1 mass concentration, highlighting the relative contributions of SO_4^{2-}, NO_3^-, and NH_4^+. (c) Total nitrate (TNO_3) and fraction between gas-phase HNO_3 and particle-phase NO_3^-. (d) Total ammonia (TNH_x) and fraction between gas-phase NH_3 and particle-phase NH_4^+. Each panel shows median values for smoke and low/no-smoke conditions separately.

https://doi.org/10.5194/egusphere-2026-4960
Preprint. Discussion started: 26 August 2026

These compositional and meteorological conditions provide the observational framework for the thermodynamic analysis that follows. Section 3.2.1 evaluates ISORROPIA-Lite model performance against observed gas-particle partitioning, and Sect. 3.2.2 presents predicted ALWC and pH across the various regions and conditions.

3.2. Thermodynamic Model Results

3.2.1. Model performance

Performance of ISORROPIA-Lite was evaluated by comparing predicted and observed gas-particle partitioning of NH_3/NH_4^+ and HNO_3/NO_3^- (expressed as $\varepsilon(NH_4^+)$ and $\varepsilon(NO_3^-)$), as well as comparing predicted and measured gas- and particle-phase concentrations for each species (Fig. 5). Additional city-level comparisons are provided in the Supplement (Sect. S2; Figs. S2-S4).

Consistent with previous work, based on its magnitude, $\varepsilon(NH_4^+)$ provides a more sensitive test of model performance than $\varepsilon(NO_3^-)$ for this dataset since partitioning coefficients are most diagnostic when ε is near 50%, where both phases are present at measurable levels. In contrast, when ε approaches 0 or 100%, one phase dominates and measurement uncertainty disproportionately affects the comparison. For AEROMMA, total ammonia was more evenly distributed between gas and particle phases (Figs. 3 and S6) whereas total nitrate was predominantly in the gas phase across all regions. Additionally, there are often less complications associated with the NH_3/NH_4^+ partitioning system. NH_4^+ is the dominant cation in PM_1 and is not present to a significant extent in coarser particles, making its prediction relatively insensitive to the measured particle size range included in the bulk analysis. From a thermodynamic view, NH_4^+ also is less sensitive to ALWC (see Discussion below). Nitrate partitioning is subject to additional complexities, including coarse-particle uptake of HNO_3, which affects measured HNO_3 and can indirectly influence equilibrium partitioning that the model does not resolve (Guo et al., 2017; Pye et al., 2020), but this effect is likely smaller for PM_1 than $PM_{2.5}$. Nitrate is also sensitive to predicted ALWC, which depends on RH and temperature uncertainties, OA concentrations (also discussed more below) and its assumed hygroscopic properties (κ_{OA}, ρ_{OA}).

https://doi.org/10.5194/egusphere-2026-4960
Preprint. Discussion started: 26 August 2026

Predicted vs measured NH_3/NH_4^+. Predicted NH_3, NH_4^+, and $\varepsilon(NH_4^+)$ were strongly correlated with the measurements ($R^2 > 0.75$) and agreed within ±10% across all flight regions and conditions (Fig. 5; Fig. S2), indicating good overall model performance. Comparisons between measured $\varepsilon(NH_4^+)$ and that predicted by Eq. (2) vs predicted pH (i.e., S curves) are shown in Fig. 8 and show good agreement. (Fig. 8 S curves are discussed in more detail later). The agreement holds under both low/no-smoke and smoke-impacted conditions (Fig. S2), supporting the predicted ALWC and pH values.

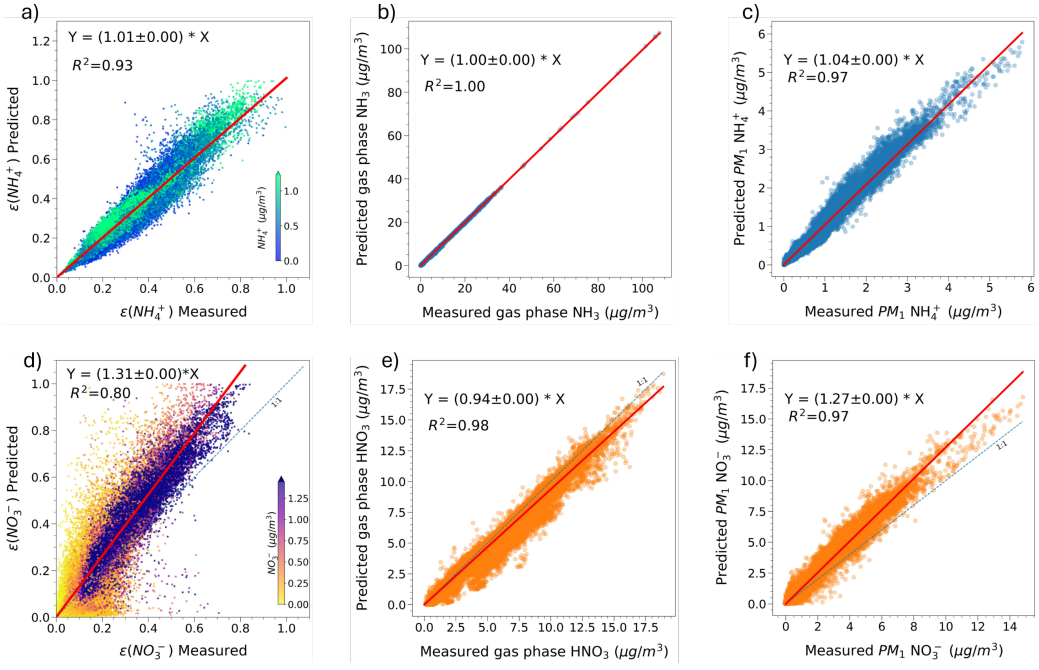

Figure 5. Comparison between ISORROPIA-Lite predicted and measured a) $\varepsilon(NH_4^+)$, b) NH_3, c) NH_4^+, d) $\varepsilon(NO_3^-)$, e) HNO_3 and f) NO_3^- for base case with OA contributions included. Data includes all boundary layer measurements used in pH predictions across all regions and conditions, excluding unique event periods. Red lines represent orthogonal distance regression fit with intercept set to 0. Slope and R^2 values are reported.

Predicted vs measured HNO_3/NO_3^-. Nitrate partitioning predictions were also highly correlated with measured values but exhibited a consistent bias (Fig. 5; Figs. S2–S5). This bias has been observed in other studies and is roughly within the combined measurement uncertainties of AMS NO_3^- (±34%) and CIMS HNO_3 (±20%), although it is systematic rather than random.

https://doi.org/10.5194/egusphere-2026-4960
Preprint. Discussion started: 26 August 2026

Specifically, on average (based on regression slopes) the model overpredicted NO_3^- and $\varepsilon(NO_3^-)$ by ~30%, while underpredicting HNO_3 by ~6%. This bias was generally consistent across all flight locations under both smoke and low/no-smoke conditions (Fig. S2). Adjusting NH_3 and HNO_3 inputs downward by their respective measurement uncertainties (12% and 20%) reduced the $\varepsilon(NO_3^-)$ bias to ~13%. A nitrate model bias of ~+30% is consistent with prior thermodynamic modeling studies utilizing different measurement techniques, and several possible explanations have been proposed. RH-dependent biases reported at low RH (<40%) in wintertime studies (Guo et al., 2016; Li et al., 2024) are not applicable here, as only data with RH > 40% (mean 65%) were retained for this analysis. Correcting for organonitrate contributions lowers measured inorganic NO_3^-, thereby worsens, rather than explain the model overprediction. Sample line heating artifacts identified in prior work did not adequately explain the bias in a past aircraft study, and including NVCs in the model worsened nitrate predictions, consistent with their minor role in PM_1 (Guo et al., 2016).

Systematic biases in temperature and RH also affect predicted partitioning and are investigated as a cause for this bias. Table S2 summarizes regression slopes and R^2 comparing ISORROPIA-Lite-predicted partitioning to measured partitioning for different model inputs. Slopes from the base case are compared to those obtained by rerunning the model with a systematic perturbation in ambient RH (scaled by a factor of 0.85) and ambient T (+0.5 °C), segregated by smoke and low/no-smoke conditions. These perturbations represent the maximum stated uncertainty for these measured parameters. For NH_3/NH_4^+, slopes changed by at most 3% for T and 12% for the RH perturbation for both smoke and low/no-smoke conditions. For HNO_3/NO_3^- partitioning, T perturbations changed slopes by up to 6%, while the RH perturbation changed slopes by up to 27% (low/no-smoke) and 35% (smoke). In all cases, R^2 showed little change. The contrasting sensitivities reflect the different thermodynamic dependencies of the two partitioning systems on ALWC. The role of RH on nitrate is explored further in Sect. 3.2.2. No single factor fully explains the bias, which likely reflects multiple compounding factors. These effects also make NO_3^- more sensitive to OA water, which is investigated next.

Role of OA water on measured vs predicted partitioning. As described in Sect. 3.1, organic aerosol is a large mass fraction of PM_1, especially during smoke events, and hence makes a significant contribution to total ALWC despite its low hygroscopicity relative to inorganic salts

https://doi.org/10.5194/egusphere-2026-4960
Preprint. Discussion started: 26 August 2026

(Table 1; Fig. 6a). Here we assess how it affects the predicted NH_3/NH_4^+ and HNO_3/NO_3^- partitioning by comparing measured partitioning with and without OA included in the thermodynamic model. Table 3 summarizes the findings for $\varepsilon(NH_4^+)$ and $\varepsilon(NO_3^-)$; Table S2 provides additional details, including comparisons of predicted and measured gas- and particle-phase species. Excluding OA reduced the slope of predicted vs measured $\varepsilon(NH_4^+)$ by ~10% and R^2 from 0.89 to 0.80 under smoke conditions (R^2 was unchanged at 0.96 when excluding OA under low/no-smoke). As expected, the model predicts less partitioning (i.e., less NH_4^+ and more gas-phase NH_3) when OA is excluded since there is less volume of water for dissolution. Similar behavior is found for $\varepsilon(NO_3^-)$, but the effect is more pronounced. As discussed above, predicted $\varepsilon(NO_3^-)$ for the combined data was consistently higher than measured partitioning, but excluding OA reduced the predicted versus measured $\varepsilon(NO_3^-)$ slope by ~30% for low/no-smoke regions and ~60% for smoke regions (or 24 and 47% respectively, for mean of differences, Table S2b), while R^2 dropped from 0.79 to 0.68 (Table 3).

Table 3. Summary of linear orthogonal distance regression (ODR; intercept = 0) slopes and (R^2) between ISORROPIA-Lite result and measured values for two ISORROPIA model configurations: including organic aerosol with inorganic species, and only inorganic species. $\varepsilon(NH_4^+)$ is $NH_4^+/(NH_4^+ + NH_3)$, $\varepsilon(NO_3^-)$ is $NO_3^-/(NO_3^- + HNO_3)$.

	$\varepsilon(NH_4^+)$		$\varepsilon(NO_3^-)$	
	With OA	Without OA	With OA	Without OA
No smoke	1.06 (0.96)	0.94 (0.96)	1.31 (0.84)	1.00 (0.82)
Smoke	0.99 (0.89)	0.89 (0.80)	1.31 (0.79)	0.69 (0.68)

These findings show the importance of OA-associated water in modulating nitrate partitioning, especially in smoke-impacted areas or in regions where emission controls have significantly reduced inorganic PM_1 relative to biogenic OA. OA water uptake is calculated using assumed constant hygroscopicity ($\kappa_{OA} = 0.1$) and density ($\rho_{OA} = 1.3$ g cm^{-3}); these parameters can vary with OA source and oxidation state, introducing additional uncertainty where OA mass is elevated. A decade-long U.S. ground-level dataset analyzed with ISORROPIA-II (which, unlike ISORROPIA-Lite, does not account for OA-associated ALWC) showed systematic underestimation of $\varepsilon(NH_4^+)$ and $\varepsilon(NO_3^-)$ under elevated biomass-burning OA (Pan et al., 2024), consistent with our findings. Including OA LWC raises predicted $\varepsilon(NO_3^-)$ and particulate NO_3^-;

https://doi.org/10.5194/egusphere-2026-4960
Preprint. Discussion started: 26 August 2026

however, if OA LWC is itself overestimated, this would propagate into an overestimate of $\varepsilon(NO_3^-)$ and NO_3^- and could account for the systematic bias we observed here.

Sensitivity of measured vs predicted partitioning on K^+ and Cl^- under smoke conditions. Water-soluble potassium, K^+, is often included under smoke conditions since it can be a significant inorganic component of fine PM. Pan et al. (2024) included K^+ in their analysis. K^+ is co-emitted with OA in biomass-burning plumes, so partitioning biases attributed to elevated OA may partly reflect K^+ influence. We do not include K^+ in our analysis, consistent with not finding increases in other inorganic species in smoke. Sensitivity tests showed that adding PILS K^+ alone worsened predictions, substantially overestimating particle-phase NH_4^+ and NO_3^- (Fig. S13). Including both PILS K^+ and Cl^- under smoke conditions had little effect (Figs. S14-S17), though $\varepsilon(NH_4^+)$ was overpredicted under low/no-smoke conditions where the presence of KCl is not expected. We performed detailed sensitivity tests with PILS-K^+ and a range of assumed K^+ and Cl^- values in Sect. S3 and find no improvement in the predicted to measured partitioning.

Overall, ISORROPIA-Lite performs well for the AEROMMA dataset. The strong NH_3/NH_4^+ agreement across all regions and conditions indicates that the bulk equilibrium assumption is valid for characterizing the inorganic thermodynamic system for the PM_1 sampled here and supports the use of predicted ALWC and pH in the analysis that follows. The persistent nitrate bias, while not substantially affecting predicted pH (given nitrate's minor role relative to sulfate across most regions in this study), needs further investigation; our sensitivity analysis suggests that a relatively small systematic high measurement bias in RH may be one possible cause.

3.2.2. Predicted ALWC and pH across urban environments

There are two main findings from the ISORROPIA-Lite predictions across the AEROMMA urban dataset. First, the aerosol was highly acidic and the pH was largely invariant: campaign-mean pH values were 1.98 ± 0.56 under low/no-smoke conditions and 2.05 ± 0.43 under smoke conditions, with 10th–90th percentile ranges of 1.5–2.5 across all urban areas regardless of smoke (or lack of smoke) concentrations (Table 1; Fig. 6b). Second, PM_1 ALWC showed considerably more variability: campaign means of 3.00 ± 6.5 μg m^{-3} (low/no-smoke) and 2.62 ± 5.5 μg m^{-3} (smoke), with substantial city-to-city differences driven primarily by RH and aerosol composition (Table 1; Fig. 6a). Because pH and ALWC are thermodynamically coupled – each

https://doi.org/10.5194/egusphere-2026-4960
Preprint. Discussion started: 26 August 2026

512 influencing the other through H^+ dilution and through compositional changes driven by gas-
513 particle partitioning of highly hygroscopic semi-volatile species – they are discussed jointly in
514 what follows, separated by smoke conditions.

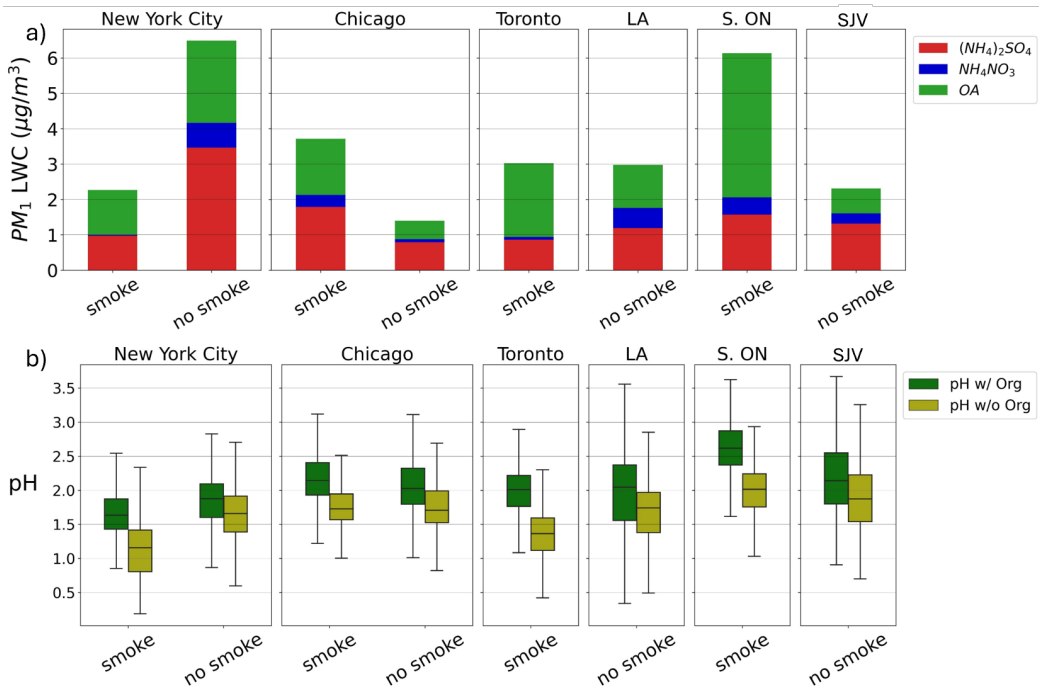

Figure 6. Species-resolved aerosol liquid water content (ALWC) and aerosol pH across AEROMMA flight regions under smoke and low/no-smoke conditions. (a) Median PM_1 ALWC partitioned into contributions from $(NH_4)_2SO_4$, NH_4NO_3, and organic aerosol (OA). (b) Aerosol pH calculated with and without OA water contributions, shown as box plots representing the 25th–75th percentile interquartile range, with whiskers extending to the 10th and 90th percentiles and the horizontal line indicating the median.

515

516 ***Low/no-smoke conditions: East–West comparison.*** PM_1 mass concentrations were 2–4×
517 higher over California compared to NYC and CHI, and PM_1 ALWC (including OA contributions)
518 also varied across both regions during low/no-smoke flights (mean ± SD: 6.19 ± 10.41 in the
519 eastern cities vs. 5.01 ± 3.79 µg m^{-3} in LA), where lower RH in California partially offset the effect
520 of higher loading of hygroscopic aerosol species (primarily NH_4NO_3) on water uptake. Across both
521 regions, $(NH_4)_2SO_4$ was the dominant contributor to inorganic ALWC, although NH_4NO_3

https://doi.org/10.5194/egusphere-2026-4960
Preprint. Discussion started: 26 August 2026

contributed more substantially over California. Mean particle pH was similar across both the eastern cities and California, with an East–West difference of only ~0.2 units (Fig. 2 and Fig. 6b), despite the large compositional contrasts, such as SO_4^{2-}/NO_3^- molar ratios of 6.17 (NYC), 5.01 (CHI), versus 1.12 (LA). This increase in nitrate fraction moving west has commonly been interpreted as evidence of substantially lower aerosol acidity in the western U.S. However, our results indicate that this compositional gradient does not result in a significant pH difference. This is consistent with the persistently low $\varepsilon(NO_3^-)$ across all regions (12 ± 12% NYC, 12 ± 10% CHI, 22 ± 14% LA).

Low/no-smoke conditions: City-level comparisons. At the city level, the contrast between NYC, CHI, and LA illustrates how RH and composition govern ALWC. Average PM_1 ALWC under low/no-smoke conditions was 10.31 ± 14.47 μg m^{-3} in NYC, 2.10 ± 1.88 in CHI, and 5.01 ± 3.79 in LA, a roughly fivefold range, yet mean pH was remarkably similar: 1.84 ± 0.33 (NYC), 2.04 ± 0.36 (CHI), and 2.09 ± 0.59 (LA) (Table 1). During low/no-smoke, $(NH_4)_2SO_4$ was the largest contributor to ALWC in all three cities; 51%, 55%, and 37% for NYC, CHI, and LA, respectively (Table 2). NH_4NO_3 played a larger role in LA (23%) than in the other cities – consistent with the higher TNO_3 and lower SO_4^{2-}/NO_3^- ratios there (Fig. 6a).

Segregating the ISORROPIA-Lite predicted ALWC by RH ranges shows that water uptake per unit mass of sulfate exceeds that of nitrate at RH below ~80%. Above 80%, nitrate uptake approaches sulfate (Fig. 7a). This is consistent with the differing hygroscopic growth factors of $(NH_4)_2SO_4$ and NH_4NO_3 as a function of RH (Tang, 1996; Zhao et al., 2021). Additionally, differences in volatility between sulfate and nitrate affect their relative contributions to ALWC. Unlike sulfate, nitrate water uptake is conditional: at a constant TNO_3, higher RH produces a different thermodynamic state with increased ALWC, higher pH through H^+ dilution, which in turn is associated with higher $\varepsilon(NO_3^-)$. This facilitates co-condensation of water and NO_3^- and further augments aerosol nitrate and its water contribution. However, this process is only significant when TNO_3 is sufficiently high. In NYC, high RH alone was insufficient to trigger substantial nitrate co-condensation given the limited TNO_3; conversely, the high TNO_3 in LA was insufficient given low RH. Correlation analysis of ALWC with individual PM_1 species mass across RH ranges confirms these dynamics (Fig. 7b): sulfate and OA correlate most strongly with ALWC at lower RH (40–70%), while nitrate shows the highest correlation at higher RH (70–85%). The RH-

https://doi.org/10.5194/egusphere-2026-4960
Preprint. Discussion started: 26 August 2026

dependent shift in nitrate contributions was more pronounced over LA than in the eastern cities due to the higher TNO_3 available there (Table S3).

The agricultural SJV region showed lower average ALWC than LA, consistent with lower PM_1 and similar RH and temperature. Mean pH in the SJV was comparable to LA, indicating that the elevated agricultural TNH_x in the SJV, almost twice that of LA, did not substantially alter aerosol acidity (Table 1). Overall, PM_1 mass was the most highly correlated to ALWC (Fig. 7b), as also found from high-spatial resolution modeling of ALWC across the continental US (Zhang et al., 2026).

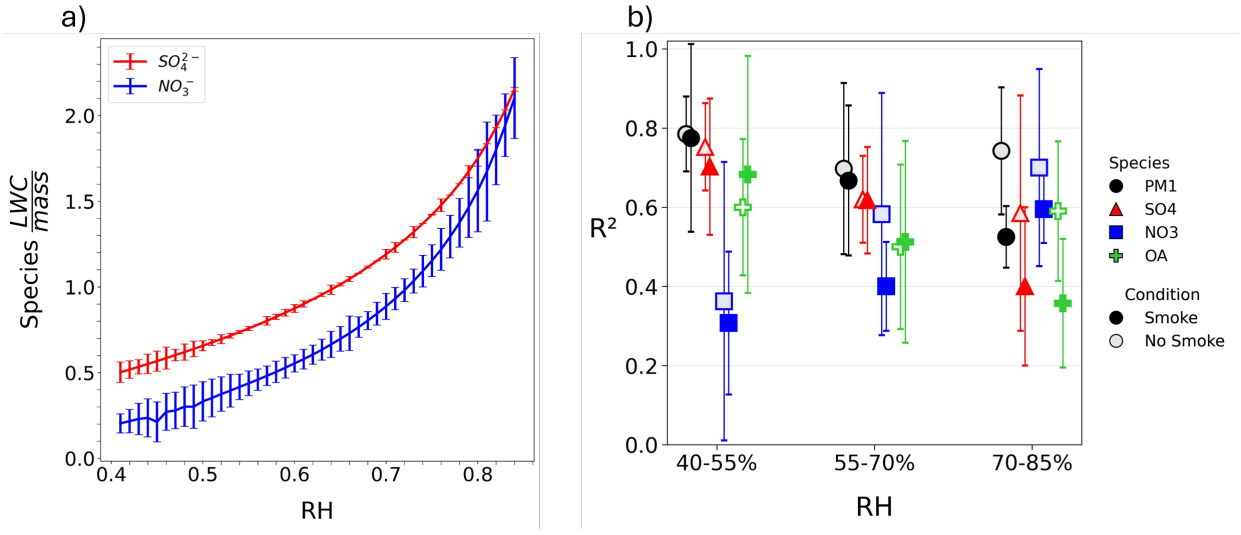

Figure 7. Sensitivity of aerosol liquid water content (ALWC) to PM_1 species mass as a function of relative humidity (RH). (a) ISORROPIA-Lite predicted water uptake per unit species mass – i.e., species-specific LWC divided by species mass – for SO_4^{2-} (red) and NO_3^- (blue) across the RH range 40–85%; error bars represent ±1 standard deviation. (b) Mean R^2 values from linear regressions between total ALWC and PM_1, SO_4^{2-}, NO_3^-, and OA mass within three RH bins (40–55%, 55–70%, and 70–85%) under smoke-impacted (filled markers) and low/no-smoke (open markers) conditions across cities; error bars represent ±1 standard deviation. Panel (a) reflects intrinsic species hygroscopicity, while panel (b) quantifies how well variations in each species' mass explain variations in total ALWC across the observed dataset.

ALWC under smoke conditions: City-level comparisons Average PM_1 ALWC predicted by the thermodynamic model during smoke-impacted flights was 3.05 ± 2.68 μg m^{-3} (NYC), 5.98 ± 11.96 (CHI), and 4.06 ± 4.77 (TO) (Table 1). The elevated OA mass under smoke conditions

https://doi.org/10.5194/egusphere-2026-4960
Preprint. Discussion started: 26 August 2026

564 increased OA LWC substantially, with OA contributing 45–65% of total ALWC across all cities,
565 up from roughly one-third under low/no-smoke conditions (Fig. 6a; Table 2). However, this
566 increase in OA LWC as a fraction of total ALWC did not scale proportionally with OA mass
567 because OA hygroscopicity (κ_{OA} = 0.1) is substantially lower than that of inorganic salts
568 (ammonium sulfate κ = 0.61, ammonium nitrate κ = 0.67) (Petters and Kreidenweis, 2007). Despite
569 OA accounting for 80–90% of total PM_1 mass during smoke flights, $(NH_4)_2SO_4$ still contributed
570 30–50% of total ALWC. NH_4NO_3, despite its hygroscopicity, contributed only 2–10% of total
571 ALWC, consistent with the persistently low aerosol-phase nitrate across all smoke-impacted cities.

572 Comparing smoke and low/no-smoke conditions at the city level shows that the net effect
573 on ALWC depended on the differences in OA and RH. In CHI, where PM_1 mass was approximately
574 three times higher during smoke flights and RH was similar, ALWC increased under smoke. In
575 NYC, where RH was approximately 24% lower during the smoke impacted period (RH=59%)
576 compared to the high-RH (83%) August 16 low/no-smoke NYC flight, RH suppression
577 outweighed the OA-driven water increase, resulting in lower mean ALWC during smoke
578 conditions. Among the three smoke-impacted cities, CHI had the highest average ALWC, ~1 μg
579 m^{-3} above TO and ~2 μg m^{-3} above NYC, consistent with its higher inorganic mass fraction
580 (especially SO_4^{2-}) and somewhat higher RH than NYC. Overall, the sensitivity of ALWC to the
581 interplay between meteorology, aerosol composition, and smoke-driven OA enhancements across
582 these cities is consistent with previous findings (Nguyen et al., 2016).

583 ***pH under smoke conditions: City level comparisons.*** Despite the substantial OA-driven
584 changes in ALWC, aerosol pH under smoke conditions remained close to values observed under
585 low/no-smoke conditions. Mean pH ranged from ~1.6 (NYC) to 2.0–2.5 (CHI) to 1.8–2.2 (TO),
586 and $\varepsilon(NO_3^-)$ remained uniformly low across all smoke-impacted cities (11–18%), with no
587 systematic smoke-related shift (Table 1; Fig. 6b). The effect of OA water on pH was more
588 pronounced under smoke than low/no-smoke conditions, consistent with the higher OA LWC
589 fractions. A maximum OA-driven pH increase of 0.62 units was observed in TO, where OA mass
590 and its contribution to ALWC were greatest. However, this represents an upper bound across the
591 dataset. Rural Southern Ontario (SON), which was also blanketed in smoke, had a similar OA
592 LWC fraction to TO but had slightly elevated pH relative to TO (2.5–3.0 vs. 1.8–2.2). This is

https://doi.org/10.5194/egusphere-2026-4960
Preprint. Discussion started: 26 August 2026

consistent with the elevated TNH_x in the rural region (~3× that of TO) and the pH-elevating influence of higher NH_3 concentrations.

The results discussed above are also evident at the within-city scale, as detailed in Sect. S1. Overall, AEROMMA pH values under both low/no-smoke and smoke conditions are consistent with previously reported summertime aerosol pH across North American urban environments (Lawal et al., 2018; Guo et al., 2017; Tao and Murphy, 2019; Arangio et al., 2022; Pan et al., 2024; Kakavas et al., 2025), reinforcing the picture of persistently acidic fine aerosol in summer with little influence from the type of wildfire smoke encountered here. Rural pH was 0.3–0.6 units higher than the surrounding urban centers where data were available, consistent with elevated agricultural NH_3.

3.2.3. Effect of OA water on pH

ISORROPIA-Lite allows predicting pH with or without OA liquid water contributions, assuming inorganic salts and hygroscopic OA are internally mixed when OA LWC is included. Table 1 summarizes the ΔpH (pH including OA LWC minus pH predicted using only inorganic species) for the various regions. OA-associated water and its effect on pH are analyzed together because they depend critically on assumed parameters and because ALWC and pH are thermodynamically linked. Recall that OA LWC was calculated using a constant hygroscopicity $\kappa_{OA} = 0.1$ and density $\rho_{OA} = 1.3$ g cm^{-3} (Petters and Kreidenweis, 2007). Under low/no-smoke conditions, OA contributed approximately one-third of total ALWC across all cities (33–38%; Table 2), and the OA-driven pH increase (ΔpH) was modest (Table 1), averaging 0.2 units campaign-wide (range 0.1–0.5 units, 10th–90th percentile). The small ΔpH under low/no-smoke conditions is consistent with the model partitioning evaluation, where including OA had no systematic effect on predicted gas-particle partitioning (Fig. 3), suggesting that $\kappa_{OA} = 0.1$ is adequate for these conditions.

Mean ΔpH under smoke conditions was higher and varied by city (0.53 ± 0.15 NYC, 0.41 ± 0.22 CHI, 0.62 ± 0.12 TO). Thus, the sensitivity of these estimates to assumed OA properties is worth noting: κ_{OA} is positively correlated with oxidation state (Jimenez et al., 2009; Massoli et al., 2010), and smoke OA may have different hygroscopicity than urban OA depending on the degree of aging. Values of ρ_{OA} and κ_{OA} predicted from O:C, H:C, and f_{CO2} derived from AMS measurements (based on Kuwata et al., 2011 and Duplissy et al., 2011) are consistently higher than

https://doi.org/10.5194/egusphere-2026-4960
Preprint. Discussion started: 26 August 2026

our assumed constant values across all areas except LA, where the two agree closely (Table S4). Note that even these predicted values may not capture the wide range of aerosol composition observed. As our approximation of constant ρ_{OA} and κ_{OA} mainly affects OA LWC, an uncertainty analysis was conducted to quantify the contribution from each of its governing factors (OA mass, κ_{OA}, ρ_{OA} and RH). Uncertainty in AMS-measured OA mass (consistent with the comparison to particle volumes discussed above) dominated the uncertainty in OA LWC, while RH uncertainty and variation in κ_{OA}, ρ_{OA} only induced small errors (Table S4). Note that because of the opposing effect of κ_{OA} and ρ_{OA} on OA LWC (direct for κ_{OA}, inverse for ρ_{OA}), using our lower values for both partially offsets their biases, further reducing the net effect on OA LWC. However, a comprehensive sensitivity analysis of these parameters under the specific OA compositions encountered during AEROMMA may be of value, but measurements of ALWC are needed to assess the importance of a more detailed analysis. Nevertheless, regardless of the exact κ_{OA} assumed, the fundamental conclusion holds; because OA hygroscopicity is substantially lower than that of inorganic sulfate, its dilution effect on pH remains modest relative to the large OA mass fractions encountered even during heavy smoke. However, OA-associated water should be included for accurate nitrate partitioning predictions under smoke conditions, as demonstrated above. The increasing contribution of wildfire smoke OA to fine PM (Burke et al., 2023) suggests that OA effects on ALWC, and pH to a lesser extent, could become more important in future.

4. DISCUSSION

4.1. Limited pH Variability

A major finding of this study is that predicted aerosol pH spanned only ~1 unit (1.5–2.5, 10th–90th percentile) despite the diverse PM_1 composition and RH encountered across the broad geographical regions and within each region (Sect. S2). (Note, T was similar throughout and RH > 40%). The broader AEROMMA dataset is consistent with a system governed by the TSO_4–TNO_3–TNH_x–H_2O system, with both TNO_3 and TNH_x contributing to pH buffering but to different extents. $\varepsilon(NO_3^-)$ was consistently low throughout the entire campaign, ranging from 0 to 0.4 across all cities and smoke conditions (Fig. 3 and S6), indicating that most TNO_3 resided in the gas phase. This $\varepsilon(NO_3^-)$ was sustained regardless of TNO_3 magnitude: even in LA, where TNO_3 substantially exceeded TNH_x by mass. Low $\varepsilon(NO_3^-)$ places all cities near the bottom flat part of the $\varepsilon(NO_3^-)$ S-curve (Fig. 8), where the HNO_3/NO_3^- system has restricted capacity to redistribute and buffer. This

https://doi.org/10.5194/egusphere-2026-4960
Preprint. Discussion started: 26 August 2026

reflects the thermodynamic properties of the HNO_3/NO_3^- couple at these summertime pH values and temperatures (i.e., $\varepsilon(NO_3^-)$) rather than reservoir (TNO_3) size. The minimal city-to-city change in $\varepsilon(NO_3^-)$ S-curve positions across conditions also confirms this (Fig. 8). In contrast, for all AEROMMA urban environments, $\varepsilon(NH_4^+)$ ranged from 0.1 to 0.7 (Fig. 3) placing all cities more on the steep central portion of its S-curve (Fig. 8), where the thermodynamic system has a greater capacity to absorb perturbations. The NH_3/NH_4^+ repartitioning therefore provides an effective pH-buffering mechanism, and explains the observed near-invariance of pH despite large differences in mass loading, ALWC, and SO_4^{2-}/NO_3^- ratios. The strong model-measurement agreement for TNH_x partitioning supports this argument. Thus, the various equilibrium states across various cities are mainly linked to the interdependence between RH, ALWC, pH, and ammonia partitioning, and to a lesser extent on nitrate partitioning, and all of which, except RH, are associated with aerosol composition. This analysis provides a thermodynamic explanation for the city-to-city $\varepsilon(NH_4^+)$ differences reported by Lill et al. (2025).

Large differences in ALWC across regions similarly did not produce proportionally large pH differences, despite ALWC being directly involved in pH (W in Eq. (1)). Even where ALWC differed by 2–3× between cities, the corresponding pH range was less than 1 unit (Table 1; Fig. 6). The net effect is that pH is buffered against ALWC variability rather than being sensitive to it.

Aerosol pH buffering has previously been explored through multiphase buffer theory (Zheng et al., 2020), which identified the NH_3/NH_4^+ system as having the highest buffering capacity among individual contributors across pH levels. Recreating this analysis for AEROMMA shows that the NH_3/NH_4^+ and HNO_3/NO_3^- systems have comparable buffering capacities in most cases, except in California under no-smoke conditions and in NYC under smoke, where NH_3/NH_4^+ dominates (Fig. S21). The buffer-capacity approach of Zheng et al. (2020) also isolates each species' individual contribution to pH buffering. As discussed above, however, these factors are interconnected in setting the equilibrium state, so isolating the effect of any single variable does not necessarily yield a representative picture of the overall buffer behavior. Since pH and ALWC are closely linked, we do not decouple ALWC buffering from the overall thermodynamic system, both are regulated together by the NH_3/NH_4^+ system, with HNO_3/NO_3^- playing a more minor role except in LA. The overall buffer behavior is better demonstrated by the ammonium and nitrate partitioning S-curves (Eqs. (2) and (3)), representing variability within each city. As shown in Fig.

https://doi.org/10.5194/egusphere-2026-4960
Preprint. Discussion started: 26 August 2026

9, as ALWC increases within a city, TNH_x and TNO_3 partition more strongly into the particle phase while the corresponding pH increase is dampened, the mean trajectories run mainly upward with increasing RH and ALWC. Although, the $\varepsilon(NH_4^+)$ and $\varepsilon(NO_3^-)$ mean trajectories are not parallel because nitrate partitioning is far more sensitive to ALWC than ammonium (Sect. 4.2). The S-curves are plotted at different ALWC values to capture the wide ALWC range in the dataset, particularly for NYC where RH spanned ~55–85%. The data points consistently track these curves, indicating NH_3/NH_4^+ and HNO_3/NO_3^- repartitioning is maintained across the full RH range sampled. Similar type behavior is seen in other locations, such as Seoul, Korea (Kim et al., 2022).

Wildfire smoke substantially increased OA and ALWC but did not significantly affect TNH_x, TNO_3, and TSO_4, preserving both the gas-phase NH_3 and HNO_3 reservoirs and their buffering capacity. Consequently, OA-associated water diluted H^+, and NH_3/NH_4^+ and HNO_3/NO_3^- repartitioning absorbs some of this perturbation. However, including OA in the thermodynamic model also perturbs inorganic ALWC – OA water alters the aqueous ionic environment (e.g., ionic strength), shifting inorganic equilibria and modifying inorganic water uptake. The interconnection between OA water uptake, inorganic equilibria, NH_3/NH_4^+ and HNO_3/NO_3^- buffering, and ALWC demonstrates the complexity of predicting aerosol pH and the necessity of a thermodynamic modeling framework that accounts for these coupled processes.

Limits on buffering are also noteworthy. For NH_3/NH_4^+, large positive perturbations in TNH_x, such as those encountered near agricultural sources, can drive pH substantially higher. The S-curves show that as pH increases $\varepsilon(NH_4^+)$ falls, and at some point TNH_x will reside almost entirely in the gas phase, the aerosol becomes more decoupled from TNH_x and further NH_3 uptake is limited. This means pH does not increase indefinitely but reaches a limit set by inorganic composition and ALWC. Because ALWC does not increase substantially under these conditions where only TNH_x is elevated, H^+ dilution is also limited, and the aerosol can remain acidic despite very elevated TNH_x. On the other hand, in cases where sufficient TNO_3 is also present, this higher-pH state couples with enhanced nitrate partitioning, greater NH_4NO_3-associated ALWC, and the secondary buffering pathway through the HNO_3/NO_3^- pair can increase in importance. Unlike $\varepsilon(NH_4^+)$, $\varepsilon(NO_3^-)$ increases with increasing pH and allows more HNO_3 to partition to the particle phase. The increased water uptake due to co-condensation with NO_3^- offsets its increased acidity (NO_3^- lowers pH and ALWC raises pH), also limiting how high pH can reach. The AEROMMA

https://doi.org/10.5194/egusphere-2026-4960
Preprint. Discussion started: 26 August 2026

urban dataset does not include this regime, $\varepsilon(NH_4^+)$ rarely approached zero and $\varepsilon(NO_3^-)$ did not approach 1, but the urban–rural pH differences observed in SJV and SON (0.3–0.6 units higher than their urban counterparts, coinciding with elevated agricultural TNH_x) are consistent with partial movement along these trajectories.

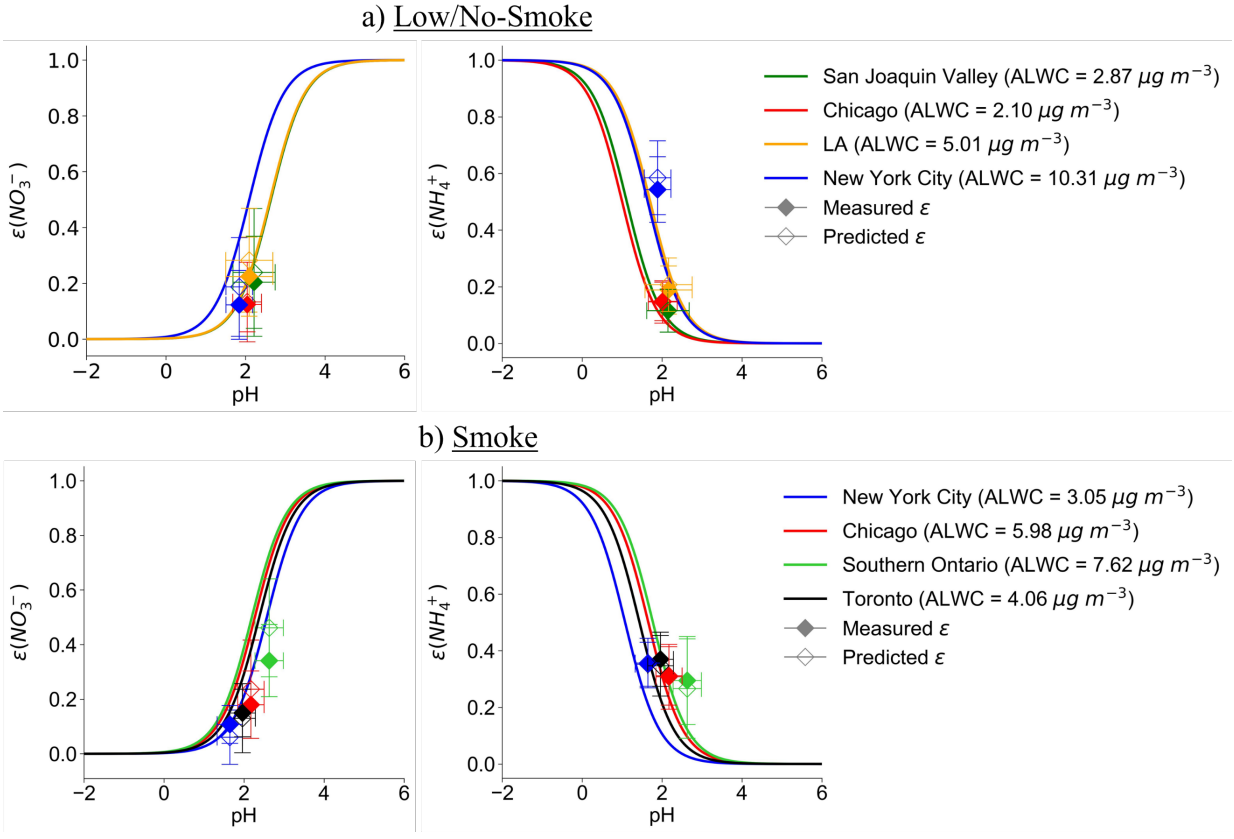

Figure 8. Theoretical ammonium and nitrate partitioning S-curves [$\varepsilon(NH_4^+)$ and $\varepsilon(NO_3^-)$ vs. pH, Equation (2) and (3)] calculated using region- and condition-specific median ALWC, temperature, and ISORROPIA-Lite-predicted activity coefficients for (a) low/no-smoke and (b) smoke flights. Left panels show nitrate partitioning $\varepsilon(NO_3^-)$ and right panels show ammonium partitioning $\varepsilon(NH_4^+)$. Filled markers indicate median measured ε, and open markers indicate mean ISORROPIA-Lite predicted ε, plotted against mean predicted pH. Error bars represent ±1 standard deviation of the data. Each curve is labeled with the corresponding region and median ALWC value.

https://doi.org/10.5194/egusphere-2026-4960
Preprint. Discussion started: 26 August 2026

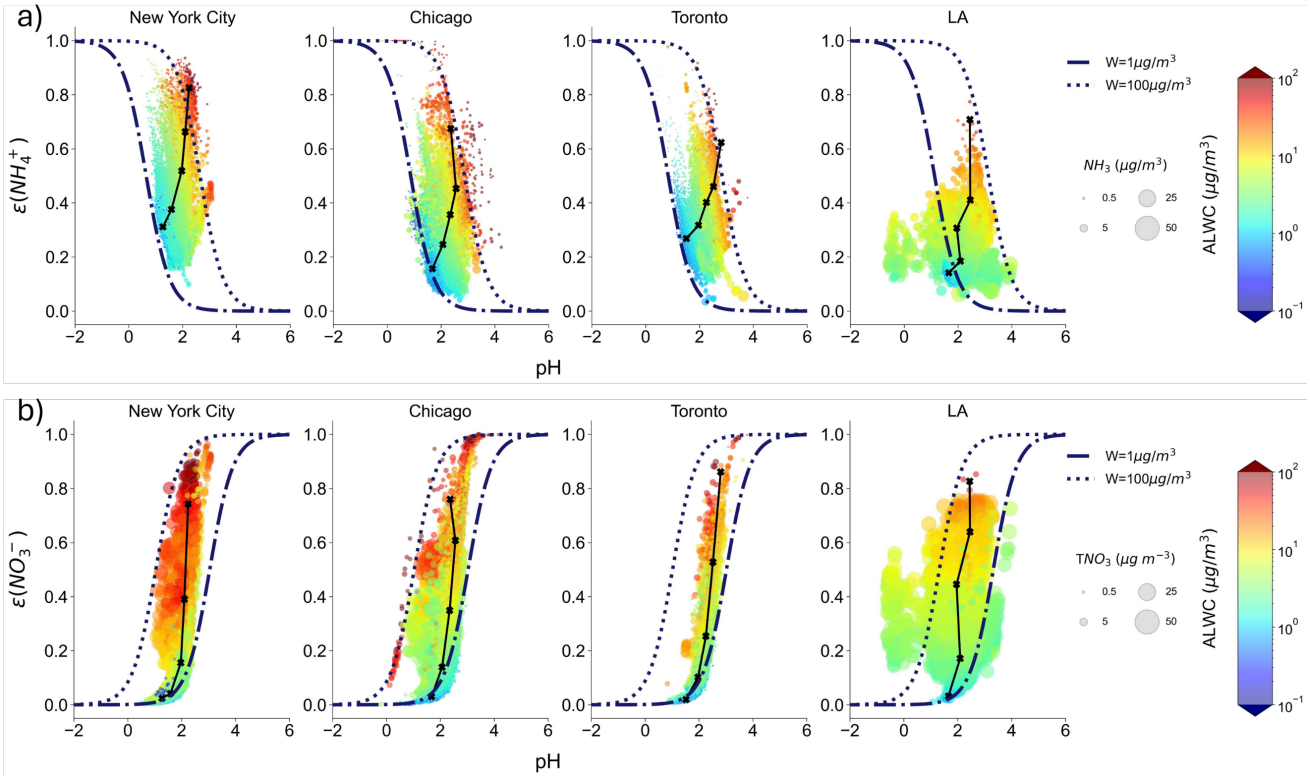

Figure 9. a) ε(NH_4^+) and b) ε(NO_3^-) as a function of aerosol pH for New York City, Chicago, Toronto, and Los Angeles, illustrating the buffering behavior of the NH_3/NH_4^+ and HNO_3/NO_3^- systems across the range of conditions sampled during AEROMMA, including both low/no-smoke and smoke conditions. Individual ISORROPIA-Lite model results are shown as scatter points colored by ALWC (μg m^{-3}, log scale) and sized by TNH_x (a) or TNO_3 (b) concentration. Theoretical S-curves calculated from Equation (2) and (3) are shown for ALWC = 1 μg m^{-3} (dot-dashed line) and ALWC = 100 μg m^{-3} (dotted line), bounding the range of liquid water conditions observed across the campaign. Black x markers denote data binned by ALWC between 0, 1, 5, 10, 50, and 100 μg m^{-3}, connected sequentially to illustrate the trajectory of ε(NH_4^+) and ε(NO_3^-) vs. pH with increasing ALWC.

718

719 **4.2. Controls on ALWC Variability and the Sensitivity of NO_3^- to ALWC**

720 While pH was near-invariant, the thermodynamic-predicted ALWC varied substantially in
721 the various regions studied. Understanding what drove this variability is of interest given ALWC's
722 role in gas–particle partitioning, control over the extent of aqueous-phase chemistry (amount of
723 aqueous reactor available), and effects on aerosol optical properties and toxicity. As shown, the

https://doi.org/10.5194/egusphere-2026-4960
Preprint. Discussion started: 26 August 2026

main controls were RH and sulfate loading, with OA contributing a secondary but important share to ALWC under smoke-impacted conditions. Nitrate's contribution to ALWC depends on the aerosol-phase NO_3^- concentration, which is determined by TNO_3 availability and thermodynamic partitioning ($\varepsilon(NO_3^-)$). Sensitivity analyses show that ISORROPIA predictions of ALWC for a given species depends on RH, demonstrated in other studies (Zhao et al., 2022); ammonium sulfate water uptake per unit mass exceeds that of ammonium nitrate at moderate RH, but ammonium nitrate's contribution to ALWC increases relative to ammonium sulfate as RH increases and can become substantial under high-TNO_3, high-RH conditions. Under these conditions, the higher ALWC, higher $\varepsilon(NO_3^-)$, and higher pH are co-determined equilibrium properties that substantially increase nitrate's contribution to ALWC relative to lower-TNO_3 or lower-RH environments. Neither the eastern cities (limited TNO_3) nor LA (low RH despite high TNO_3) displayed this co-condensation effect to a significant extent during AEROMMA, so nitrate's contribution to ALWC remained minor. In principle, high-TNO_3, high-RH conditions, which are more common in winter at lower temperatures, could place the system in a nitrate-driven ALWC regime.

We have shown that the thermodynamic model predicts NO_3^- to be far more sensitive than NH_4^+ to changes in ALWC, a difference with important implications that we now examine in more detail. It arises in part from the opposite dependencies of the anion and cation equilibria on aqueous-phase H^+, which become apparent when concentrations are expressed per volume of air rather than as aqueous-phase molar concentrations. Assuming ideal solutions, the equilibrium expressions for anions (e.g., NO_3^-) and cations (e.g., NH_4^+) have a different dependence on ALWC. The air-equivalent concentration of NO_3^- scales with the square of ALWC, while that of NH_4^+ has no dependence on ALWC. For the anion, the ALWC dependence is from both the conversion from aqueous-to-air concentrations and the conversion of $[H^+]_{aq}$ *to* $[H^+]_{air}$, producing a quadratic dependence. For the cation, these two ALWC factors cancel, since $[H^+]_{aq}$ appears in the numerator of the corresponding aqueous-phase expression. This sensitivity also applies to $\varepsilon(NO_3^-)$ being far more sensitive than $\varepsilon(NH_4^+)$ to ALWC, since the denominators in each partitioning expression (TNO_3 and TNH_x) are fixed by ambient conditions. A more detailed derivation is provided in Sect. S4.

The dependence of NH_4^+ on H^+_{air} and lack of a ALWC dependence is consistent with the often-cited role of NH_4^+ as the primary aerosol cation balancing the charge of SO_4^{2-} and NO_3^-. The particle-phase charge balance gives $H^+_{air} \approx 2[SO_4^{2-}] + [NO_3^-] - [NH_4^+]$ (molar concentrations in

https://doi.org/10.5194/egusphere-2026-4960
Preprint. Discussion started: 26 August 2026

air, moles per cubic meter), which is consistent with the observed high correlations among these species (Fig. S1a and S1b). The equality is approximate because it omits possible other ions (e.g., bisulfate (HSO_4^-), which is included in the ISOROPPIA calculation of H^+_{air}). It should be noted that this analysis only qualitatively shows the contrast in ALWC sensitivity; it does not give quantitative predictions of the ALWC dependences since fine PM are not ideal due to high ionic strengths which will affect the dependence on ALWC through activity coefficients.

This difference in sensitivity to ALWC has implications for model performance (as shown in Sect. 3.2.1). Errors or biases in ALWC, arising, for example, from uncertainties in RH or other factors affecting ALWC, or neglecting OA liquid water, will disproportionately affect predicted NO_3^- relative to NH_4^+. The dependence of NO_3^- on ALWC also means that OA liquid water, even when it represents only a minor fraction of total ALWC, can influence particulate NO_3^- and aerosol pH if NO_3^- is a significant component, as discussed above. The bias we observed in this study, also seen in other studies, where the model predicts higher $\varepsilon(NO_3^-)$ and NO_3^- then measured may be due to an over prediction of ALWC.

4.3. The Role of Temperature

Aerosol thermodynamics are strongly temperature dependent. Lower temperatures reduce the equilibrium vapor pressures of semi-volatile species, shifting gas–particle partitioning toward the condensed phase through increased Henry's law constants, modified dissociation equilibrium constants for condensed-phase species, and changes in activity coefficients. Temperature was not highly variable across the measurement regions in this study and therefore was not associated with significant variability in ALWC or pH, allowing the analysis to focus on the effects of composition and RH.

The pH and buffering behaviors described above are specific to daytime summer conditions. While AEROMMA had no nighttime flights that met our analysis conditions (RH > 40%), lower temperatures at night and in cooler seasons shift thermodynamic equilibria toward the condensed phase, with similar effects on ALWC and pH. This temperature driven shift toward condensed-phase partitioning has been shown to result in substantially higher fine-particle NO_3^- concentrations in winter (Guo et al., 2016; Tao and Murphy, 2019) and at night (Guo et al., 2015). The associated thermodynamic state, characterized by elevated ALWC driven by NH_4NO_3 water uptake and higher aerosol pH, represents a different regime from the sulfate-dominated, low-nitrate

https://doi.org/10.5194/egusphere-2026-4960
Preprint. Discussion started: 26 August 2026

daytime summer conditions sampled during AEROMMA. NH_3/NH_4^+ buffering is also temperature sensitive: the partitioning S-curves shift toward higher pH at lower temperatures (Guo et al., 2017; Campbell et al., 2024), which would further modulate pH responses in colder months and at night. Extending the AEROMMA-style analysis to winter campaigns and nighttime sampling would be valuable for testing whether the TSO_4–TNH_x–H_2O system that primarily governs daytime summer aerosol acidity transitions to a more nitrate-active regime, and for evaluating thermodynamic model performance under those contrasting conditions.

4.4. Lack of Smoke influence on AEROMMA inorganic species

Fine aerosols in fresh smoke plumes are known to contain inorganic aerosol species, including TNH_x and K^+, that can raise pH (Cahill et al., 2008; Pye et al., 2020). The absence of substantial smoke-driven pH increases during AEROMMA contrasts with conditions of fresh smoke plumes in general and prior observations of long-range biomass burning plumes measured over the Eastern Mediterranean, where aerosol pH was ~1 unit higher than background conditions (Bougiatioti et al., 2016). The key distinction with AEROMMA is that smoke originating primarily from Northwest Territories wildfires and likely more than two days old at the time of sampling (Jain et al., 2024; Lill et al., 2025) was diluted, and its minor inorganic constituents (SO_4^{2-}, NO_3^-, NH_4^+, K^+) did not cause a significant perturbation when mixed with urban emissions that are themselves sources of most of these species. In contrast, smoke in the Eastern Mediterranean study produced clear shifts in inorganic composition relative to no-smoke conditions: lower sulfate (~1.5×), substantially elevated NO_3^- (2–6×), and high $\varepsilon(NO_3^-)$ (65 ± 14% vs. ~20% under non-smoke conditions), indicating that smoke there perturbed the inorganic system. OA, however, which is a dominant smoke component produced a clear enhancement in PM_1 mass in both places. This view of diluted smoke with minor inorganic PM_1 species during AEROMMA is confirmed by measurements of smoke in the free troposphere above TO, which show that the smoke prior to mixing into the urban boundary layer was not significantly enhanced in inorganic species (see Sect. S5 for a detailed analysis).

5. IMPLICATIONS AND SUMMARY

These findings have important environmental implications due to their effects that include PM_1 mass and reactive nitrogen deposition. The thermodynamics strongly favored gas-phase HNO_3 with consistently low $\varepsilon(NO_3^-)$ of 10–22% across all cities meaning aerosol-phase nitrate

https://doi.org/10.5194/egusphere-2026-4960
Preprint. Discussion started: 26 August 2026

was weakly coupled to TNO_3 concentrations under summer conditions. Despite similar $\varepsilon(NO_3^-)$ between cities, LA aerosol nitrate loadings were 3–10 times greater than eastern cities mainly because TNO_3 was 2–8 times higher, a mass-driven rather than acidity-driven difference. This sensitivity has direct relevance for emission controls. Because $\varepsilon(NO_3^-)$ lies in a relatively pH-insensitive range under current summer conditions, controls aimed at reduction of PM_1 NO_3^-, through lowering TNO_3 (i.e., NO_x emission or oxidant controls) translate to only marginal reductions in aerosol nitrate (NO_3^- = $\varepsilon(NO_3^-)$ x TNO_3). However, a PM_1 pH increase of ~1 unit would shift $\varepsilon(NO_3^-)$ beyond ~50%, substantially amplifying the aerosol nitrate response to changes in TNO_3 level. The city-to-city range in $\varepsilon(NH_4^+)$, from ~17% in CHI and LA to ~56% in NYC, was affected by differences in ALWC and pH (Fig. 8). This demonstrates that despite the low molecular weight of ammonia, its contribution to PM_1 mass is sensitive to meteorological conditions even when aerosol acidity is fairly uniform across cities. Emission control strategies targeting NH_3 reductions will therefore be more effective than HNO_3 controls, although with regionally variable effects depending on factors that control the pH-ALWC system (e.g., RH, sulfate, TNH_x). Consistent with these findings, rural areas sampled during AEROMMA had pH values approximately 0.3–0.6 units higher than the surrounding urban centers, coinciding with elevated agricultural NH_3.

The predominance of gas-phase oxidized nitrogen during AEROMMA has significant implications for reactive nitrogen deposition and ecosystem impacts (Baker et al., 2021; Nenes et al., 2021). The low $\varepsilon(NO_3^-)$ indicates that oxidized reactive nitrogen under summer conditions is susceptible to rapid dry deposition near emission sources, given the substantially higher deposition velocities of gas-phase HNO_3 relative to PM_1 NO_3^-. Under conditions favoring greater particle-phase partitioning, higher RH, lower temperatures, or elevated TNH_x near agricultural sources that raises pH and $\varepsilon(NO_3^-)$ and $\varepsilon(NH_4^+)$, reactive nitrogen would instead be retained in the aerosol phase and transported farther before deposition, with downstream consequences for soil chemistry, water quality, and nitrogen-sensitive ecosystems. The pH buffering described above moderates the magnitude of these partitioning shifts in response to meteorological and the atmospheric composition (TSO_4, TNO_3, TNH_x, and OA), underscoring the importance of accurately representing aerosol pH and ALWC in deposition and chemical transport models.

The low aerosol pH (1.5–2.5) and its persistence across diverse conditions also has important implications for aerosol chemistry, toxicity, and health. Lower ALWC over California,

https://doi.org/10.5194/egusphere-2026-4960
Preprint. Discussion started: 26 August 2026

driven by low RH despite high PM_1 mass, suggests more limited aqueous-phase processing relative to eastern cities. Inorganic species substantially influenced ALWC throughout the study (Fig. 6a), implying that the inorganic thermodynamic system still plays a role in aqueous-phase reaction pathways even under the high-OA smoke impacted conditions examined here. The sustained pH range of 1.5–2.5 promotes acid-catalyzed reactions including organosulfate formation and IEPOX uptake (Jang et al., 2002; Lei et al., 2022) and sustains conditions favorable for the dissolution of redox-active trace metals such as Fe and Cu, whose solubility increases exponentially below pH ~3 (Fang et al., 2017). Elevated oxidative potential from metal dissolution is therefore a persistent feature of North American urban fine aerosol in summer, largely unperturbed by the large compositional and meteorological variability observed. The principal exception is near agricultural sources, where elevated NH_3 locally raises pH and may attenuate these chemistry and toxicity pathways. The finding that aged wildfire smoke of the type encountered during AEROMMA did not substantially alter this pH regime is notable given growing concerns about smoke-driven aerosol toxicity. However, this result cannot be generalized to fresher or enriched plumes more enriched in inorganic species, which will produce a different aerosol thermodynamic equilibrium state.

The principal findings of this study are:

- **Persistently low, near-invariant pH.** Predicted PM_1 pH stayed within 1.5–2.5 (10th–90th percentile, mean ~2) across all four cities, despite the East–West compositional gradient, smoke and low/no-smoke conditions, and a roughly fivefold range in ALWC.
- **A coupled system controls pH, not any single species.** NH_3/NH_4^+ lies on the steep part of its partitioning S-curve and buffers effectively, whereas HNO_3/NO_3^- lies on or near the flat, low-ε portion with limited redistribution capacity; pH is governed by the coupled TSO_4–TNO_3–TNH_x–H_2O system. To understand aerosol acidity, the complete thermodynamic system must be solved.
- **Partitioning validates the model, but there is a nitrate bias.** Predicted $\varepsilon(NH_4^+)$ agreed with observations ($R^2 > 0.75$, within ~±10%), whereas $\varepsilon(NO_3^-)$ and NO_3^- were systematically overpredicted by ~30% on average; this bias does not significantly affect predicted pH given nitrate's minor role and may, in part, be related to uncertainties in ALWC.

https://doi.org/10.5194/egusphere-2026-4960
Preprint. Discussion started: 26 August 2026

- **OA water dominates ALWC under smoke but barely shifts pH.** Inorganic ions dominate ALWC outside smoke despite representing less than 30% of total PM_1; within smoke, OA water is 45–65% of ALWC, yet pH rose by ≤0.62 units because OA hygroscopicity ($\kappa_{OA} \approx 0.1$) is significantly below that of sulfate. Including OA water, however, improved predictions of nitrate partitioning.
- **Nitrate is much more sensitive to ALWC than ammonium.** Air-equivalent NO_3^- scales approximately with $ALWC^2$ while NH_4^+ is independent of ALWC, so errors in ALWC (from RH or OA water) propagate disproportionately into predicted NO_3^- and likely contribute to the nitrate bias.
- **The East–West nitrate gradient is mass-driven, not acidity-driven.** Higher PM_1 nitrate in Los Angeles reflects the 2–8× higher TNO_3 rather than lower pH (the East–West pH difference is only ~0.2 units); the historical interpretation of this gradient as an acidity gradient is not supported.
- **Aged wildfire smoke left the inorganic thermodynamics unchanged.** Diluted, >2 day-old smoke raised OA and ALWC but not TSO_4, TNO_3, TNH_x, or pH, in contrast to fresh or inorganic-enriched plumes; the result was that smoke did not significantly change pH, but it did affect ALWC.
- **Implications.** Low $\varepsilon(NO_3^-)$ keeps oxidized nitrogen largely gaseous, favoring rapid near-source dry deposition; NH_3 controls are more effective than HNO_3 controls for summertime PM_1 nitrate; and a sustained pH of 1.5–2.5 maintains acid-catalyzed chemistry and trace-metal (Fe, Cu) dissolution, with agricultural NH_3 the main exception.

Data and Code Availability Statement : AEROMMA data are publicly available in the archives at https://doi.org/10.25921/079X-9716. ISORROPIA-Lite is available at https://github.com/EPFL-LAPI/ISORROPIA-Iite.

https://doi.org/10.5194/egusphere-2026-4960
Preprint. Discussion started: 26 August 2026

Author Contributions: MM and RW designed the research component of this paper, interpreted the results and wrote the paper. AS, AP, SA, AM, WC, AR, SB, CW, EL, IP, LX, KB, JC and PW collected and processed the observational datasets used in this study. MM performed model simulations and visualized the data. SK, SP and AN developed the model code. All authors reviewed the paper.

Competing interests: At least one of the (co-)authors is a member of the editorial board of Atmospheric Chemistry and Physics.

Acknowledgements: MM and RW were funded by the U.S. National Oceanic and Atmospheric Administration grant no. NA21OAR4310126-T1-01. The Caltech group was supported by NASA 80NSSC21K1704. KB was also supported by a NASA FINESST fellowship 80NSSC24K0005. CIRES researchers were supported by the NOAA cooperative agreement NA22OAR4320151.
We thank the entire AEROMMA science team for their contributions to the campaign, the pilots and flight crew of the NASA DC-8 for their role in obtaining the measurements. We also thank the instrument supervisors and their teams: Emily Fischer for the ammonia data, Glenn Diskin for the relative humidity data, Joshua Schwarz and Georgia Michailoudi for the black carbon measurements, Charles Brock for the particle volume data, and the CH_3CN measurement team (Matt Coggon (NOAA CSL), Chelsea E. Stockwell (NOAA CSL), Kelvin H. Bates (NOAA CSL and CIRES at UC Boulder, now at Dept. Mech. E. UC Boulder), and Georgios Gkatzelis (Forschungszentrum Jülich).

https://doi.org/10.5194/egusphere-2026-4960
Preprint. Discussion started: 26 August 2026

Reference

Arangio, A. M., Shahpoury, P., Dabek-Zlotorzynska, E., and Nenes, A.: Seasonal Aerosol Acidity, Liquid Water Content and Their Impact on Fine Urban Aerosol in SE Canada, Atmosphere, 13, 1012, https://doi.org/10.3390/atmos13071012, 2022.

Bahreini, R., Ervens, B., Middlebrook, A. M., Warneke, C., de Gouw, J. A., DeCarlo, P. F., Jimenez, J. L., Brock, C. A., Neuman, J. A., Ryerson, T. B., Stark, H., Atlas, E., Brioude, J., Fried, A., Holloway, J. S., Peischl, J., Richter, D., Walega, J., Weibring, P., Wollny, A. G., and Fehsenfeld, F. C.: Organic aerosol formation in urban and industrial plumes near Houston and Dallas, Texas, Journal of Geophysical Research: Atmospheres, 114, https://doi.org/10.1029/2008JD011493, 2009.

Baker, A. R., Kanakidou, M., Nenes, A., Myriokefalitakis, S., Croot, P. L., Duce, R. A., Gao, Y., Guieu, C., Ito, A., Jickells, T. D., Mahowald, N. M., Middag, R., Perron, M. M. G., Sarin, M. M., Shelley, R., and Turner, D. R.: Changing atmospheric acidity as a modulator of nutrient deposition and ocean biogeochemistry, Science Advances, 7, eabd8800, https://doi.org/10.1126/sciadv.abd8800, 2021.

Bougiatioti, A., Nikolaou, P., Stavroulas, I., Kouvarakis, G., Weber, R., Nenes, A., Kanakidou, M., and Mihalopoulos, N.: Particle water and pH in the eastern Mediterranean: source variability and implications for nutrient availability, Atmospheric Chemistry and Physics, 16, 4579–4591, https://doi.org/10.5194/acp-16-4579-2016, 2016.

Burke, M., Childs, M. L., de la Cuesta, B., Qiu, M., Li, J., Gould, C. F., Heft-Neal, S., and Wara, M.: The contribution of wildfire to PM2.5 trends in the USA, Nature, 622, 761–766, https://doi.org/10.1038/s41586-023-06522-6, 2023.

Cahill, C. F., Cahill, T. A., and Perry, K. D.: The size- and time-resolved composition of aerosols from a sub-Arctic boreal forest prescribed burn, Atmospheric Environment, 42, 7553–7559, https://doi.org/10.1016/j.atmosenv.2008.04.034, 2008.

Campbell, J. R., Battaglia, M., Dingilian, K. K., Cesler-Maloney, M., Simpson, W. R., Robinson, E. S., DeCarlo, P. F., Temime-Roussel, B., D'Anna, B., Holen, A. L., Wu, J., Pratt, K. A., Dibb, J. E., Nenes, A., Weber, R. J., and Mao, J.: Enhanced aqueous formation and

https://doi.org/10.5194/egusphere-2026-4960
Preprint. Discussion started: 26 August 2026

neutralization of fine atmospheric particles driven by extreme cold, Science Advances, 10, eado4373, https://doi.org/10.1126/sciadv.ado4373, 2024.

Chace, W. S., Womack, C., Ball, K., Bates, K. H., Bohn, B., Coggon, M., Crounse, J. D., Fuchs, H., Gilman, J., Gkatzelis, G. I., Jernigan, C. M., Novak, G. A., Novelli, A., Peischl, J., Pollack, I., Robinson, M. A., Rollins, A., Schafer, N. B., Schwantes, R. H., Selby, M., Stainsby, A., Stockwell, C., Taylor, R., Treadaway, V., Veres, P. R., Warneke, C., Waxman, E., Wennberg, P. O., Wolfe, G. M., Xu, L., Zuraski, K., and Brown, S. S.: Ozone Production Efficiencies in the Three Largest United States Cities from Airborne Measurements, Environ. Sci. Technol., 59, 13306–13318, https://doi.org/10.1021/acs.est.5c02073, 2025.

Chen, J.-H., Puttu, U., Huynh, H. N., Ahern, A. T., Ball, K., Bates, K. H., Brock, C. A., Campos, T., Coggon, M. M., Crounse, J. D., de Gouw, J., DiGangi, J. P., Diskin, G. S., Gkatzelis, G. I., Halliday, H. S., Hu, L., Koss, A. R., Li, Y., Lyu, M., Michailoudi, G., Murphy, S. M., Nowak, J. B., Palm, B. B., Peischl, J., Permar, W., Perring, A. E., Pokhrel, R. P., Schafer, N. B., Schwarz, J. P., Sekimoto, K., Selimovic, V., Stockwell, C. E., Sullivan, A. P., Thornton, J. A., Wagner, N. L., Wang, S., Warneke, C., Wennberg, P. O., Zeng, L., Yokelson, R. J., Weber, R. J., and Xu, L.: Atmospheric Evolution of Brown Carbon from Wildfires in North America, Environ. Sci. Technol., 59, 17145–17159, https://doi.org/10.1021/acs.est.5c09020, 2025.

Crounse, J. D., McKinney, K. A., Kwan, A. J., and Wennberg, P. O.: Measurement of Gas-Phase Hydroperoxides by Chemical Ionization Mass Spectrometry, Anal. Chem., 78, 6726–6732, https://doi.org/10.1021/ac0604235, 2006.

DeCarlo, P. F., Kimmel, J. R., Trimborn, A., Northway, M. J., Jayne, J. T., Aiken, A. C., Gonin, M., Fuhrer, K., Horvath, T., Docherty, K. S., Worsnop, D. R., and Jimenez, J. L.: Field-Deployable, High-Resolution, Time-of-Flight Aerosol Mass Spectrometer, Anal. Chem., 78, 8281–8289, https://doi.org/10.1021/ac061249n, 2006.

Duplissy, J., DeCarlo, P. F., Dommen, J., Alfarra, M. R., Metzger, A., Barmpadimos, I., Prevot, A. S. H., Weingartner, E., Tritscher, T., Gysel, M., Aiken, A. C., Jimenez, J. L., Canagaratna, M. R., Worsnop, D. R., Collins, D. R., Tomlinson, J., and Baltensperger, U.: Relating

https://doi.org/10.5194/egusphere-2026-4960
Preprint. Discussion started: 26 August 2026

hygroscopicity and composition of organic aerosol particulate matter, Atmospheric Chemistry and Physics, 11, 1155–1165, https://doi.org/10.5194/acp-11-1155-2011, 2011.

Fang, T., Guo, H., Zeng, L., Verma, V., Nenes, A., and Weber, R. J.: Highly Acidic Ambient Particles, Soluble Metals, and Oxidative Potential: A Link between Sulfate and Aerosol Toxicity, Environ. Sci. Technol., 51, 2611–2620, https://doi.org/10.1021/acs.est.6b06151, 2017.

Fountoukis, C. and Nenes, A.: ISORROPIA II: a computationally efficient thermodynamic equilibrium model for K^+–Ca^{2+}–Mg^{2+}–NH_4^+–Na^+–SO_4^{2-}–NO_3^-–Cl^-–H_2O aerosols, Atmospheric Chemistry and Physics, 7, 4639–4659, https://doi.org/10.5194/acp-7-4639-2007, 2007.

Fountoukis, C., Nenes, A., Sullivan, A., Weber, R., Van Reken, T., Fischer, M., Matías, E., Moya, M., Farmer, D., and Cohen, R. C.: Thermodynamic characterization of Mexico City aerosol during MILAGRO 2006, Atmospheric Chemistry and Physics, 9, 2141–2156, https://doi.org/10.5194/acp-9-2141-2009, 2009.

Guo, H., Xu, L., Bougiatioti, A., Cerully, K. M., Capps, S. L., Hite, J. R. J., Carlton, A. G., Lee, S.-H., Bergin, M. H., Ng, N. L., Nenes, A., and Weber, R. J.: Fine-particle water and pH in the southeastern United States, Atmospheric Chemistry and Physics, 15, 5211–5228, https://doi.org/10.5194/acp-15-5211-2015, 2015.

Guo, H., Sullivan, A. P., Campuzano-Jost, P., Schroder, J. C., Lopez-Hilfiker, F. D., Dibb, J. E., Jimenez, J. L., Thornton, J. A., Brown, S. S., Nenes, A., and Weber, R. J.: Fine particle pH and the partitioning of nitric acid during winter in the northeastern United States, Journal of Geophysical Research: Atmospheres, 121, 10,355-10,376, https://doi.org/10.1002/2016JD025311, 2016.

Guo, H., Liu, J., Froyd, K. D., Roberts, J. M., Veres, P. R., Hayes, P. L., Jimenez, J. L., Nenes, A., and Weber, R. J.: Fine particle pH and gas–particle phase partitioning of inorganic species in Pasadena, California, during the 2010 CalNex campaign, Atmospheric Chemistry and Physics, 17, 5703–5719, https://doi.org/10.5194/acp-17-5703-2017, 2017.

https://doi.org/10.5194/egusphere-2026-4960
Preprint. Discussion started: 26 August 2026

Guo, H., Campuzano-Jost, P., Nault, B. A., Day, D. A., Schroder, J. C., Kim, D., Dibb, J. E., Dollner, M., Weinzierl, B., and Jimenez, J. L.: The importance of size ranges in aerosol instrument intercomparisons: a case study for the Atmospheric Tomography Mission, Atmospheric Measurement Techniques, 14, 3631–3655, https://doi.org/10.5194/amt-14-3631-2021, 2021.

Hand, J. L., Schichtel, B. A., Pitchford, M., Malm, W. C., and Frank, N. H.: Seasonal composition of remote and urban fine particulate matter in the United States, Journal of Geophysical Research: Atmospheres, 117, https://doi.org/10.1029/2011JD017122, 2012.

Harrison, R. M. and Yin, J.: Particulate matter in the atmosphere: which particle properties are important for its effects on health?, Science of The Total Environment, 249, 85–101, https://doi.org/10.1016/S0048-9697(99)00513-6, 2000.

Hennigan, C. J., Izumi, J., Sullivan, A. P., Weber, R. J., and Nenes, A.: A critical evaluation of proxy methods used to estimate the acidity of atmospheric particles, Atmospheric Chemistry and Physics, 15, 2775–2790, https://doi.org/10.5194/acp-15-2775-2015, 2015.

Hennigan, C. J., McKee, M., Pratap, V., Boegner, B., Reno, J., Garcia, L., McLaren, M., and Lance, S. M.: pH dependence of brown-carbon optical properties in cloud water, Atmospheric Chemistry and Physics, 23, 14437–14449, https://doi.org/10.5194/acp-23-14437-2023, 2023.

Jain, P., Barber, Q. E., Taylor, S. W., Whitman, E., Castellanos Acuna, D., Boulanger, Y., Chavardès, R. D., Chen, J., Englefield, P., Flannigan, M., Girardin, M. P., Hanes, C. C., Little, J., Morrison, K., Skakun, R. S., Thompson, D. K., Wang, X., and Parisien, M.-A.: Drivers and Impacts of the Record-Breaking 2023 Wildfire Season in Canada, Nat Commun, 15, 6764, https://doi.org/10.1038/s41467-024-51154-7, 2024.

Jang, M., Czoschke, N. M., Lee, S., and Kamens, R. M.: Heterogeneous Atmospheric Aerosol Production by Acid-Catalyzed Particle-Phase Reactions, Science, 298, 814–817, https://doi.org/10.1126/science.1075798, 2002.

Jimenez, J. L., Canagaratna, M. R., Donahue, N. M., Prevot, A. S. H., Zhang, Q., Kroll, J. H., DeCarlo, P. F., Allan, J. D., Coe, H., Ng, N. L., Aiken, A. C., Docherty, K. S., Ulbrich, I. M., Grieshop, A. P., Robinson, A. L., Duplissy, J., Smith, J. D., Wilson, K. R., Lanz, V. A.,

https://doi.org/10.5194/egusphere-2026-4960
Preprint. Discussion started: 26 August 2026

Hueglin, C., Sun, Y. L., Tian, J., Laaksonen, A., Raatikainen, T., Rautiainen, J., Vaattovaara, P., Ehn, M., Kulmala, M., Tomlinson, J. M., Collins, D. R., Cubison, M. J., E., Dunlea, J., Huffman, J. A., Onasch, T. B., Alfarra, M. R., Williams, P. I., Bower, K., Kondo, Y., Schneider, J., Drewnick, F., Borrmann, S., Weimer, S., Demerjian, K., Salcedo, D., Cottrell, L., Griffin, R., Takami, A., Miyoshi, T., Hatakeyama, S., Shimono, A., Sun, J. Y., Zhang, Y. M., Dzepina, K., Kimmel, J. R., Sueper, D., Jayne, J. T., Herndon, S. C., Trimborn, A. M., Williams, L. R., Wood, E. C., Middlebrook, A. M., Kolb, C. E., Baltensperger, U., and Worsnop, D. R.: Evolution of Organic Aerosols in the Atmosphere, Science, 326, 1525–1529, https://doi.org/10.1126/science.1180353, 2009.

Kakavas, S., Pandis, S. N., and Nenes, A.: ISORROPIA-Lite: A Comprehensive Atmospheric Aerosol Thermodynamics Module for Earth System Models, Tellus B: Chemical and Physical Meteorology, 74, 1, https://doi.org/10.16993/tellusb.33, 2022.

Kakavas, S., Siouti, E., Nenes, A., and Pandis, S. N.: Effects of wind-blown dust emissions on size-resolved aerosol acidity over the US, Atmospheric Environment, 345, 121056, https://doi.org/10.1016/j.atmosenv.2025.121056, 2025.

Kim, Y., Park, O., Park, S. H., Kim, M. J., Kim, J.-J., Choi, J.-Y., Lee, D., Cho, S., and Shim, S.: PM2.5 pH estimation in Seoul during the KORUS-AQ campaign using different thermodynamic models, Atmospheric Environment, 268, 118787, https://doi.org/10.1016/j.atmosenv.2021.118787, 2022.

Klein, L. K., Luo, B., Bluvshtein, N., Krieger, U. K., Schaub, A., Glas, I., David, S. C., Violaki, K., Motos, G., Pohl, M. O., Hugentobler, W., Nenes, A., Stertz, S., Peter, T., and Kohn, T.: Expiratory aerosol pH is determined by indoor room trace gases and particle size, Proceedings of the National Academy of Sciences, 119, e2212140119, https://doi.org/10.1073/pnas.2212140119, 2022.

Kuwata, M., Zorn, S. R., and Martin, S. T.: Using Elemental Ratios to Predict the Density of Organic Material Composed of Carbon, Hydrogen, and Oxygen, Environ. Sci. Technol., 46, 787–794, https://doi.org/10.1021/es202525q, 2011.

Lawal, A. S., Guan, X., Liu, C., Henneman, L. R. F., Vasilakos, P., Bhogineni, V., Weber, R. J., Nenes, A., and Russell, A. G.: Linked Response of Aerosol Acidity and Ammonia to SO2

https://doi.org/10.5194/egusphere-2026-4960
Preprint. Discussion started: 26 August 2026

and NOx Emissions Reductions in the United States, Environ. Sci. Technol., 52, 9861–9873, https://doi.org/10.1021/acs.est.8b00711, 2018.

Lei, Z., Chen, Y., Zhang, Y., Cooke, M. E., Ledsky, I. R., Armstrong, N. C., Olson, N. E., Zhang, Z., Gold, A., Surratt, J. D., and Ault, A. P.: Initial pH Governs Secondary Organic Aerosol Phase State and Morphology after Uptake of Isoprene Epoxydiols (IEPOX), Environ. Sci. Technol., 56, 10596–10607, https://doi.org/10.1021/acs.est.2c01579, 2022.

Li, E., Pierce, J. R., Juncosa Calahorrano, J. F., Sullivan, A. P., Pollack, I. B., Roscioli, J. R., Caulton, D. R., McCabe, M. E., Jathar, S. H., and Fischer, E. V.: Inorganic Nitrogen Gas-Aerosol Partitioning in and Around Animal Feeding Operations in Northeastern Colorado in Late Summer 2021, Journal of Geophysical Research: Atmospheres, 129, e2023JD040507, https://doi.org/10.1029/2023JD040507, 2024.

Li, G., Su, H., Zheng, G., Zhou, M., Han, W., Zhang, Y., Ma, N., Wang, H., Klimach, T., and Cheng, Y.: Novel Device for in Situ and Real-Time Detection of the Acidity of Ambient Aerosols: Laboratory Characterization and Ambient Measurements, Environ. Sci. Technol., 59, 659–667, https://doi.org/10.1021/acs.est.4c09221, 2025.

Liao, H. and Seinfeld, J. H.: Global impacts of gas-phase chemistry-aerosol interactions on direct radiative forcing by anthropogenic aerosols and ozone, Journal of Geophysical Research: Atmospheres, 110, https://doi.org/10.1029/2005JD005907, 2005.

Lill, E. R., Pollack, I. B., Roscioli, J. R., Middlebrook, A. M., Piasecki, A., Albertin, S., Carlson, S., Sullivan, A., Schafer, N., Peischl, J., Rollins, A., Waxman, E. M., Zuraski, K., Gilman, J. B., Treadaway, V., Selby, M., Stockwell, C. E., Coggon, M. M., Bates, K. H., Warneke, C., Pierce, J. R., and Fischer, E. V.: Ammonia Observations Over Large North American Cities, Journal of Geophysical Research: Atmospheres, 130, e2025JD044019, https://doi.org/10.1029/2025JD044019, 2025.

Luo, B., Schaub, A., Glas, I., Klein, L. K., David, S. C., Bluvshtein, N., Violaki, K., Motos, G., Pohl, M. O., Hugentobler, W., Nenes, A., Krieger, U. K., Stertz, S., Peter, T., and Kohn, T.: Expiratory Aerosol pH: The Overlooked Driver of Airborne Virus Inactivation, Environ. Sci. Technol., 57, 486–497, https://doi.org/10.1021/acs.est.2c05777, 2023.

https://doi.org/10.5194/egusphere-2026-4960
Preprint. Discussion started: 26 August 2026

Massoli, P., Lambe, A. T., Ahern, A. T., Williams, L. R., Ehn, M., Mikkilä, J., Canagaratna, M. R., Brune, W. H., Onasch, T. B., Jayne, J. T., Petäjä, T., Kulmala, M., Laaksonen, A., Kolb, C. E., Davidovits, P., and Worsnop, D. R.: Relationship between aerosol oxidation level and hygroscopic properties of laboratory generated secondary organic aerosol (SOA) particles, Geophysical Research Letters, 37, https://doi.org/10.1029/2010GL045258, 2010.

Meskhidze, N., Chameides, W. L., Nenes, A., and Chen, G.: Iron mobilization in mineral dust: Can anthropogenic SO2 emissions affect ocean productivity?, Geophysical Research Letters, 30, https://doi.org/10.1029/2003GL018035, 2003.

Middlebrook, A. M., Bahreini, R., Jimenez, J. L., and Canagaratna, M. R.: Evaluation of Composition-Dependent Collection Efficiencies for the Aerodyne Aerosol Mass Spectrometer using Field Data, Aerosol Science and Technology, 46, 258–271, https://doi.org/10.1080/02786826.2011.620041, 2012.

Nah, T., Guo, H., Sullivan, A. P., Chen, Y., Tanner, D. J., Nenes, A., Russell, A., Ng, N. L., Huey, L. G., and Weber, R. J.: Characterization of aerosol composition, aerosol acidity, and organic acid partitioning at an agriculturally intensive rural southeastern US site, Atmospheric Chemistry and Physics, 18, 11471–11491, https://doi.org/10.5194/acp-18-11471-2018, 2018.

Nenes, A., Pandis, S. N., Weber, R. J., and Russell, A.: Aerosol pH and liquid water content determine when particulate matter is sensitive to ammonia and nitrate availability, Atmospheric Chemistry and Physics, 20, 3249–3258, https://doi.org/10.5194/acp-20-3249-2020, 2020.

Nenes, A., Pandis, S. N., Kanakidou, M., Russell, A. G., Song, S., Vasilakos, P., and Weber, R. J.: Aerosol acidity and liquid water content regulate the dry deposition of inorganic reactive nitrogen, Atmospheric Chemistry and Physics, 21, 6023–6033, https://doi.org/10.5194/acp-21-6023-2021, 2021.

Nguyen, T. K. V., Capps, S. L., and Carlton, A. G.: Decreasing Aerosol Water Is Consistent with OC Trends in the Southeast U.S., Environ. Sci. Technol., 49, 7843–7850, https://doi.org/10.1021/acs.est.5b00828, 2015.

https://doi.org/10.5194/egusphere-2026-4960
Preprint. Discussion started: 26 August 2026

Nguyen, T. K. V., Zhang, Q., Jimenez, J. L., Pike, M., and Carlton, A. G.: Liquid Water: Ubiquitous Contributor to Aerosol Mass, Environ. Sci. Technol. Lett., 3, 257–263, https://doi.org/10.1021/acs.estlett.6b00167, 2016.

Oakes, M., Ingall, E. D., Lai, B., Shafer, M. M., Hays, M. D., Liu, Z. G., Russell, A. G., and Weber, R. J.: Iron Solubility Related to Particle Sulfur Content in Source Emission and Ambient Fine Particles, Environ. Sci. Technol., 46, 6637–6644, https://doi.org/10.1021/es300701c, 2012.

Pan, D., Mauzerall, D. L., Wang, R., Guo, X., Puchalski, M., Guo, Y., Song, S., Tong, D., Sullivan, A. P., Schichtel, B. A., Collett, J. L., and Zondlo, M. A.: Regime shift in secondary inorganic aerosol formation and nitrogen deposition in the rural United States, Nat. Geosci., 17, 617–623, https://doi.org/10.1038/s41561-024-01455-9, 2024.

Petters, M. D. and Kreidenweis, S. M.: A single parameter representation of hygroscopic growth and cloud condensation nucleus activity, Atmospheric Chemistry and Physics, 7, 1961–1971, https://doi.org/10.5194/acp-7-1961-2007, 2007.

Phillips, S. M., Bellcross, A. D., and Smith, G. D.: Light Absorption by Brown Carbon in the Southeastern United States is pH-dependent, Environ. Sci. Technol., 51, 6782–6790, https://doi.org/10.1021/acs.est.7b01116, 2017.

Pilinis, C., Seinfeld, J. H., and Grosjean, D.: Water content of atmospheric aerosols, Atmospheric Environment (1967), 23, 1601–1606, https://doi.org/10.1016/0004-6981(89)90419-8, 1989.

Pollack, I. B., Lindaas, J., Roscioli, J. R., Agnese, M., Permar, W., Hu, L., and Fischer, E. V.: Evaluation of ambient ammonia measurements from a research aircraft using a closed-path QC-TILDAS operated with active continuous passivation, Atmospheric Measurement Techniques, 12, 3717–3742, https://doi.org/10.5194/amt-12-3717-2019, 2019.

Pye, H. O. T., Nenes, A., Alexander, B., Ault, A. P., Barth, M. C., Clegg, S. L., Collett Jr., J. L., Fahey, K. M., Hennigan, C. J., Herrmann, H., Kanakidou, M., Kelly, J. T., Ku, I.-T., McNeill, V. F., Riemer, N., Schaefer, T., Shi, G., Tilgner, A., Walker, J. T., Wang, T., Weber,

https://doi.org/10.5194/egusphere-2026-4960
Preprint. Discussion started: 26 August 2026

R., Xing, J., Zaveri, R. A., and Zuend, A.: The acidity of atmospheric particles and clouds, Atmos. Chem. Phys., 20, 4809–4888, https://doi.org/10.5194/acp-20-4809-2020, 2020.

Reid, J. S., Koppmann, R., Eck, T. F., and Eleuterio, D. P.: A review of biomass burning emissions part II: intensive physical properties of biomass burning particles, Atmospheric Chemistry and Physics, 5, 799–825, https://doi.org/10.5194/acp-5-799-2005, 2005.

Song, X., Wu, D., Su, Y., Li, Y., and Li, Q.: Review of health effects driven by aerosol acidity: Occurrence and implications for air pollution control, Science of The Total Environment, 955, 176839, https://doi.org/10.1016/j.scitotenv.2024.176839, 2024.

Surratt, J. D., Lewandowski, M., Offenberg, J. H., Jaoui, M., Kleindienst, T. E., Edney, E. O., and Seinfeld, J. H.: Effect of Acidity on Secondary Organic Aerosol Formation from Isoprene, Environ. Sci. Technol., 41, 5363–5369, https://doi.org/10.1021/es0704176, 2007.

Tang, I. N.: Chemical and size effects of hygroscopic aerosols on light scattering coefficients, Journal of Geophysical Research: Atmospheres, 101, 19245–19250, https://doi.org/10.1029/96JD03003, 1996.

Tanner, R. L., Olszyna, K. J., Edgerton, E. S., Knipping, E., and Shaw, S. L.: Searching for evidence of acid-catalyzed enhancement of secondary organic aerosol formation using ambient aerosol data, Atmospheric Environment, 43, 3440–3444, https://doi.org/10.1016/j.atmosenv.2009.03.045, 2009.

Tao, Y. and Murphy, J. G.: The sensitivity of $PM_{2.5}$ acidity to meteorological parameters and chemical composition changes: 10-year records from six Canadian monitoring sites, Atmospheric Chemistry and Physics, 19, 9309–9320, https://doi.org/10.5194/acp-19-9309-2019, 2019.

Tilgner, A., Schaefer, T., Alexander, B., Barth, M., Collett Jr., J. L., Fahey, K. M., Nenes, A., Pye, H. O. T., Herrmann, H., and McNeill, V. F.: Acidity and the multiphase chemistry of atmospheric aqueous particles and clouds, Atmospheric Chemistry and Physics, 21, 13483–13536, https://doi.org/10.5194/acp-21-13483-2021, 2021.

https://doi.org/10.5194/egusphere-2026-4960
Preprint. Discussion started: 26 August 2026

Weber, R. J., Guo, H., Russell, A. G., and Nenes, A.: High aerosol acidity despite declining atmospheric sulfate concentrations over the past 15 years, Nature Geosci, 9, 282–285, https://doi.org/10.1038/ngeo2665, 2016.

Zhang, B., Yin, L., Yang, Y., Guo, H., Xu, L., Di, Q., Wei, Y., Wei, J., Pan, D., Schwartz, J., Ng, N. L., Weber, R. J., and Liu, P.: High-resolution aerosol liquid water content in the contiguous United States using machine learning, npj Clim Atmos Sci, https://doi.org/10.1038/s41612-026-01371-2, 2026.

Zhao, P., Ge, S., Su, J., Ding, J., and Kuang, Y.: Relative Humidity Dependence of Hygroscopicity Parameter of Ambient Aerosols, Journal of Geophysical Research: Atmospheres, 127, e2021JD035647, https://doi.org/10.1029/2021JD035647, 2022.

Zheng, G., Su, H., Wang, S., Andreae, M. O., Pöschl, U., and Cheng, Y.: Multiphase buffer theory explains contrasts in atmospheric aerosol acidity, Science, 369, 1374–1377, https://doi.org/10.1126/science.aba3719, 2020.